NASA/CR–2016-219170

Refined AFC-Enabled High-Lift System Integration Study

Peter M. Hartwich, Arvin Shmilovich, Douglas S. Lacy, Eric D. Dickey,
Anthony J. Scalafani, P. Sundaram, and Yoram Yadlin
The Boeing Company, Huntington Beach, California

March 2016

NASA STI Program . . . in Profile

Since its founding, NASA has been dedicated to the advancement of aeronautics and space science. The NASA scientific and technical information (STI) program plays a key part in helping NASA maintain this important role.

The NASA STI program operates under the auspices of the Agency Chief Information Officer. It collects, organizes, provides for archiving, and disseminates NASA's STI. The NASA STI program provides access to the NTRS Registered and its public interface, the NASA Technical Reports Server, thus providing one of the largest collections of aeronautical and space science STI in the world. Results are published in both non-NASA channels and by NASA in the NASA STI Report Series, which includes the following report types:

- TECHNICAL PUBLICATION. Reports of completed research or a major significant phase of research that present the results of NASA Programs and include extensive data or theoretical analysis. Includes compilations of significant scientific and technical data and information deemed to be of continuing reference value. NASA counter-part of peer-reviewed formal professional papers but has less stringent limitations on manuscript length and extent of graphic presentations.

- TECHNICAL MEMORANDUM. Scientific and technical findings that are preliminary or of specialized interest, e.g., quick release reports, working papers, and bibliographies that contain minimal annotation. Does not contain extensive analysis.

- CONTRACTOR REPORT. Scientific and technical findings by NASA-sponsored contractors and grantees.

- CONFERENCE PUBLICATION. Collected papers from scientific and technical conferences, symposia, seminars, or other meetings sponsored or co-sponsored by NASA.

- SPECIAL PUBLICATION. Scientific, technical, or historical information from NASA programs, projects, and missions, often concerned with subjects having substantial public interest.

- TECHNICAL TRANSLATION. English-language translations of foreign scientific and technical material pertinent to NASA's mission.

Specialized services also include organizing and publishing research results, distributing specialized research announcements and feeds, providing information desk and personal search support, and enabling data exchange services.

For more information about the NASA STI program, see the following:

- Access the NASA STI program home page at http://www.sti.nasa.gov

- E-mail your question to help@sti.nasa.gov

- Phone the NASA STI Information Desk at 757-864-9658

- Write to:
  NASA STI Information Desk
  Mail Stop 148
  NASA Langley Research Center
  Hampton, VA 23681-2199

NASA/CR–2016-219170

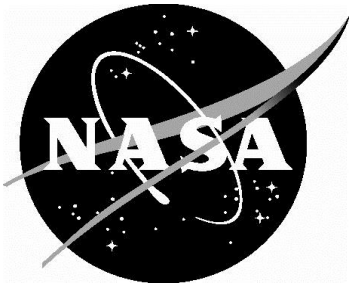

Refined AFC-Enabled High-Lift System Integration Study

Peter M. Hartwich, Arvin Shmilovich, Douglas S. Lacy, Eric D. Dickey,
Anthony J. Scalafani, P. Sundaram, and Yoram Yadlin
The Boeing Company, Huntington Beach, California

National Aeronautics and
Space Administration

Langley Research Center
Hampton, Virginia 23681-2199

Prepared for Langley Research Center
under Contract NNL14AB98T

March 2016

Available from:

NASA STI Program/Mail Stop 148
NASA Langlet Research Center
Hampton, Virginia 23681-2199
Fax: 757-864-6500

Acknowledgments

This study was carried out under NASA Contract: NNL10AA05B / NNL14AB98T. Dr. John C. Lin was the NASA LaRC Task Principal Investigator. In addition to the authors, the following Boeing personnel contributed to this work: W. Burggraf, P. Camacho, K. El-Gohary, A.B. Gonzales, and E.L. Lawson.

Abstract

A prior trade study established the effectiveness of using Active Flow Control (AFC) for reducing the mechanical complexities associated with a modern high-lift system without sacrificing aerodynamic performance at low-speed flight conditions representative of takeoff and landing. The current technical report expands on this prior work in two ways: (1) a refined conventional high-lift system based on the NASA Common Research Model (CRM) is presented that is more representative of modern commercial transport aircraft in terms of stall characteristics and maximum Lift/Drag (L/D) ratios at takeoff and landing-approach flight conditions; and (2) the design trade space for AFC-enabled high-lift systems is expanded to explore a wider range of options for improving their efficiency.

The refined conventional high-lift CRM (HL-CRM) concept features leading edge slats and slotted trailing edge flaps with Fowler motion. For the current AFC-enhanced high lift system trade study, the refined conventional high-lift system is simplified by substituting simply-hinged trailing edge flaps for the slotted single-element flaps with Fowler motion.

The high-lift performance of these two high-lift CRM variants is established using Computational Fluid Dynamics (CFD) solutions to the Reynolds-Averaged Navier-Stokes (RANS) equations. These CFD assessments identify the high-lift performance that needs to be recovered through AFC to have the CRM variant with the lighter and mechanically simpler high-lift system match the performance of the conventional high-lift system.

In parallel to the conventional high-lift concept development, parametric studies using CFD guided the development of an effective and efficient AFC-enabled simplified high-lift system. This included parametric trailing edge flap geometry studies addressing the effects of flap chord length and flap deflection. As for the AFC implementation, scaling effects (i.e., wind-tunnel versus full-scale flight conditions) are addressed, as are AFC architecture aspects such as AFC unit placement, number AFC units, operating pressures, mass flow rates, and steady versus unsteady AFC applications. These efforts led to the development of a novel traversing AFC actuation concept which is efficient in that it reduces the AFC mass flow requirements by as much as an order of magnitude compared to previous AFC technologies, and it is predicted to be effective in driving the aerodynamic performance of a mechanical simplified high-lift system close to that of the reference conventional high-lift system.

Conceptual system integration studies were conducted for the AFC-enhanced high-lift concept applied to a NASA Environmentally Responsible Aircraft (ERA) reference configuration, the so-called ERA-0003 concept. The results from these design integration assessments identify overall system performance improvement opportunities over conventional high-lift systems that suggest the viability of further technology maturation efforts for AFC-enabled high lift flap systems. To that end, technical challenges are identified associated with the application of AFC-enabled high-lift systems to modern transonic commercial transports for future technology maturation efforts.

Nomenclature

α	Angle of attack
AFC	Active Flow Control
AFRL	Air Force Research Laboratory
AIAA	American Institute of Aeronautics & Astronautics
APU	Auxiliary Power Unit
ATT	Advanced Tactical Theater
CFD	Computational Fluid Dynamics
CRM	Common Research Model
DLR	Deutsche Luft & Raumfahrt (German Air & Space)
ERA	Environmentally Responsible Aircraft
LE	Leading edge
MADCAP	Modular Aerodynamic Computational Analysis Process
NFAC	National Full Scale Aerodynamic Complex
NPV	Net Present Value
OEW	Overall Empty Weight
QFD	Quality Function Deployment
RANS	Reynolds-Averaged Navier–Stokes
TE	Trailing edge
TOD	Takeoff Distance
TOFL	Takeoff Field Length
TOGW	Takeoff Gross Weight
TRL	Technical Readiness Level
WACC	Weighted Average Cost of Capital
WUSS	Wing Under Slat Surface

CONTENTS

1.0 INTRODUCTION

Modern high-lift systems are designed to allow a transport aircraft - with typical transonic cruise speeds - to safely operate at slow speeds for landing and takeoff operations. The high lift system is usually slotted both on the leading edge and the trailing edge of the wing to take advantage of the aerodynamic properties of slotted flows and achieve the necessary high lift performance. The slotted leading and trailing edge devices, and the associated sub-system necessary to change the wing configuration from cruise to low-speed, are complex and employ a significant number of parts to enable safe operation. In addition, these complex mechanical high-lift systems often protrude externally under the wings - and require external fairings - that result in increased cruise drag.

McLean et al. [1] explored a range of active flow control (AFC) applications for improving the efficiency of next-generation commercial transonic transport aircraft. They identified AFC-enhanced simplified high-lift systems as a high payoff / high risk technology for reducing weight and fuel consumption for the targeted aircraft class. The rationale was that AFC would remedy flow separations that are anticipated when typical high-lift systems would be replaced with mechanically simpler and lighter variants.

Since that McLean report, much research has been directed at exploring the capabilities and limitations of AFC applications to simplifed high lift systems, starting with computational and experimental studies on two-dimensional airfoils [2], then to full-scale vertical tails [3], and finally a flight demonstration [4].

The latter application of AFC to the vertical tail of a B757 aircraft motivated a series exploratory AFC-enabled high lift system integration studies. To explain, one could think of the AFC-augmented B757 vertical tail as a wing with a simply hinged trailing edge flap where AFC deployment increases high lift performance instead of improving rudder control effectiveness. The results from a pilot trade study on AFC-enabled high-lift systems [5] demonstrated the effectiveness of such systems while it also indicated a need for further design integration studies to address inefficiencies in the initial AFC high-lift system concepts. The AFC power requirements were such that the associated system trade studies failed to produce a technically feasible and economically viable conceptual aircraft design solution.

The current technical report aims at addressing these and other shortcomings in that exploratory AFC-enabled high-lift system integration study. The conventional high-lift system based on the NASA Common Research Model (CRM) was modified to produce stall behavior and maximum Lift/Drag (L/D) ratios at takeoff and landing-approach flight conditions that are representative of modern commercial transport. In parallel, the design trade space for AFC-enabled high-lift systems is expanded to explore options for improving their efficiency.

Next, two refined high-lift concepts based on the Common Research Model (CRM) outer mold line (OML) definition will be presented. One represents a refinement of an existing conventional high-lift Common Research Model (CRM) draft concept featuring leading edge slats and slotted trailing edge flaps with Fowler motion. Its geometrically simpler sibling enhanced by AFC is realized by substituting simply hinged for the slotted trailing edge flaps. The relative high-lift performance of these two high-lift CRM variants is established using Computational Fluid Dynamics (CFD) solutions to the Reynolds-Averaged Navier-Stokes (RANS) equations for steady

flow. These CFD results identify the loss in aerodynamic performance due to the mechanically simpler trailing–edge high-lift system that needs to be recovered through AFC.

The geometric sizing and deployment of the simply hinged flap, along with its AFC system integration solution is based on parametric studies, including scaling effects (i.e., wind-tunnel versus full-scale flight conditions), AFC unit placement, number AFC units, operating pressures, mass flow rates, and steady versus unsteady AFC applications.

The impact of an AFC-enhanced high-lift system on the overall aircraft performance is assessed by performance trades on a reference aircraft concept, assuming either a conventional or and AFC-enhanced simplified high-lift system. This project element aims at the identification of any weight and fuel savings due to a simplified AFC-augmented high-lift system that would translate into a positive net present value (NPV).

At the conclusion of the current study, technical challenges of AFC-enabled high-lift systems for modern transonic commercial transports are identified for future technology maturation efforts.

2.0 CONVENTIONAL AND AFC-ENABLED HIGH LIFT SYSTEM DEVELOPMENT

As discussed by Lacy and Sclafani [6], the availability of geometry of relevant commercial transport high lift configurations in the public domain usually falls into two categories: dated aerodynamics (e.g., wing or high lift device sections) on a relevant planform or potentially relevant aerodynamics on a planform not representative of a commercial transport (e.g., simple low aspect ratio trapezoidal wing). This triggered a Boeing-internal design effort to fill this void by creating a set of relevant high lift geometry that can be made available in the public domain for, for instance, high lift technology, with the performance levels achieved by the geometry serving as benchmarks for a conventional high lift system.

The previously released cruise speed CRM definition [7, 8] provides a useful and logical springboard for this effort, as it is a wing/body/horizontal/nacelle/pylon geometry set representative of a generic long range, twin engine configuration. For this effort to produce a high lift geometry set, each portion of the cruise geometry was re-evaluated for its suitability for this role. For all elements, the goal was for the result to be representative of a modern commercial airplane.

2.1 Conventional High-Lift CRM (HL-CRM) Configuration

While it was desired to maintain as much similarity to the existing high speed CRM wing geometry as possible, the CRM wing was re-lofted to achieve a spanwise straightening for easier implementation of the high-lift devices, and the leading-edge curvature was modified to make it more amenable to low-speed operation; this is illustrated in Figure 1.

The primary leading edge device types in use on jet transports today are slats, rigid Kruegers, variable camber Kruegers and a simple drooped leading edge. For outboard wings (outboard of the nacelle), far and away the most common device is the slat, which is actuated forward and nose down to enable desired positioning relative to the Wing Under Slat Surface (WUSS), the designed main wing element leading edge surface that is covered by the slat when it is stowed for cruise. For inboard leading edges, more options have historically been utilized. With slats

still being the mostly chosen option, slats were chosen for the HL-CRM inboard and outboard wing sections.

There were two objectives for the leading edge design. First was to enable the wing to reach sufficiently high angles of attack for takeoff and landing configurations to achieve representative performance levels. The second was for the airplane to pitch nose down at stall to aid in stall recovery. Satisfying the first goal can be achieved through a combination of providing sufficient slat chord across the span and defining suitable slat positioning and WUSS designs. Satisfying the second goal requires one to manage the relative health of the inboard and outboard wing regions near stall. In order to get pitch down at stall, the inboard wing must stall first. These desires coupled with an assessment of the range of chord versus span from a collection of existing airplanes led to the decision to choose a constant chord slat over the inboard span, and distribution of chord over the outboard span that tapers down linearly from the nacelle location to the wing tip. The final slat chord distribution is shown plotted with the range of slat sizing from previous airplanes in Figure 2.

Two deployed slat positions are provided for the HL-CRM. The fully extended position is referred to as the landing position (30° slat deflection), while the intermediate position will be used for takeoff (22° slat deflection). Many recent transports configured with slats employ a circular arc trajectory between the stowed and deployed positions. For enhanced realism, this has been used as a constraint for the HL-CRM as well. While it is possible to employ a different axis of rotation for each individual slat panel, a single axis has been defined for the whole inboard slat span and another axis has been defined for the entire outboard slat span. This was done for simplicity as well as to enable flexibility in possible future slat segmentation decisions. It should also be noted that both the takeoff and landing slat positions employ a gap between the slat upper surface trailing edge and WUSS. This was mostly done to ease grid generation for Computational Fluid Dynamics (CFD) analyses.

There was an attempt to maintain as much realism in the constraints of the slat and WUSS surfaces as possible. A sufficient distance between the slat leading edge and the WUSS leading edge was maintained for structural viability reasons. In addition, the WUSS upper surface was designed assuming a thinner, more realistic slat trailing edge thickness. However, the actual upper and lower slat trailing edge thicknesses have been opened up to 0.20” full scale for wind tunnel model viability by altering the inner slat cove surface. As a result, wind tunnel model slats built with these definitions cannot be stowed due to interference (see Figure 3). This is not deemed to be an issue as separate cruise leading edge parts can be built to test the stowed slat configuration.

Single-slotted flaps have become the norm for new commercial transport aircraft. Reduced complexity and weight, cost and lower noise are but a few reasons for this trend. Therefore, single-slotted flaps were chosen for the HL-CRM trailing edge. As with the leading edge, a distribution of device chord needed to be chosen, and as with the slats, device sizing from existing jet transport airplanes was examined for guidance. Based on these data, flap chord across the outboard flap was chosen to be 25% of local wing chord. For the inboard flap, a constant chord across the span was chosen that was equal to the chord of the outboard flap at its inboard end. As can be seen in Figure 4, this chord distribution falls in the middle of the historical data.

The other key variable to establish is the location of the spoiler-trailing-edge (or fixed-trailing-edge in regions of flap span without spoilers) relative to the flap. The further aft on the flap that this is, the more aft translation (Fowler motion) that results as the flap deploys. The

spoiler trailing edge was placed at 40% of flap chord for the HL-CRM, a value representative of typical commercial transports.

Due to the fact that the wing was sheared to produce straight upper surface span lines in the vicinity of the stowed slat trailing edge, a fair amount of curvature in rear view exists in the curve representing the spoiler trailing edge, relative to which the flap gap is measured. This characteristic tends to drive the configuration toward non-linear spanwise gap distributions, with larger than desired gaps in the mid-span regions of the flaps. To combat this tendency, the stowed flap leading edge was pushed forward somewhat in the middle of both flap elements relative to the chord definition specified above. Through this chord modification and flap shape tailoring across the span, the design goal was achieved. This is illustrated for the outboard flap in the 25° (takeoff) and 37° (landing approach) position in Figure 5, which shows how the flap leading edge tracks the spoiler trailing edge to provide uniform gap distributions.

The high speed CRM was configured with a flow-through fan cowl that was attached to the wing with a pylon. The initial objective was to simply position this existing nacelle and pylon on the new wing for the HL-CRM using the same methodology as used to position it previously on the high speed CRM wing. While this is essentially what was done, it was also determined that the pylon intersection with the wing lower surface extended aft onto the lower surface of the stowed flap. To simplify flaps-down modeling, the pylon was shortened by 12 inches so that it closed out ahead of the stowed flap leading edge. The modification was all done aft of the point of maximum thickness of the pylon and is expected to have minimal effect on the aerodynamic performance at low speeds.

2.2 Simplified High-Lift CRM Configuration

The main difference between the so-called conventional high-lift CRM concept and its pendant with a (mechanically) simplified high-lift system is found in the trailing-edge flap design. There, the single slotted inboard and outboard flaps with a Fowler motion for the conventional high-lift CRM concept are replaced with simply hinged flaps. Figure 6 shows a detail of the simply-hinged trailing edge flap design in a three-quarter rear view.

3.0 CFD-BASED ASSESSMENTS OF HIGH-LIFT AERODYNAMICS

Computational Fluid Dynamics (CFD) was used to estimate the performance of both conventional and simplified HL-CRM concepts by exercising two established flow solvers: CFD++ and OVERFLOW. These are widely used Reynolds-Averaged Navier-Stokes (RANS) codes considered reliable and accurate for analyzing modern transport configurations at or near a design condition for both cruise and high-lift configurations. Evaluating general aerodynamic characteristics of the HL-CRM using two different methods allows for increased confidence that the overall design is generally acceptable.

3.1 Computational Grids

The CFD++ flow solver is run on unstructured computational grids. To illustrate such unstructured grids, details of the anisotropic tetrahedral mesh of the conventional HL-CRM in nominal takeoff configuration are shown in Figures 7 and 8. Figure 8 also gives an example of the careful attention given to refining wake regions. It is because of details like these that the overall mesh consists of more than 186 million cells.

The HL-CRM structured, overset grid system was constructed under the general guidelines established for the 1st High Lift Prediction Workshop (HiLiftPW) [9, 10]. The surface grid to-

pology for the landing configuration is shown in Figure 9. This image is intended to illustrate the general layout of the various grids that define the major airplane components such as the flaps. The geometry in this figure is defined by the surface mesh that, in some areas, is so dense it appears to be a solid surface. The grid is made-up of 86.6 million points. Again, much care was applied to resolving the viscous wake regions as illustrated in Figure 10 which shows a planar slice through the volume grid in the mid-span wing region.

3.2 Flow Solver Specifications

The CFD++ flow solver is a widely used general purpose RANS code that is compatible with both structured and unstructured grids including overset and hybrid. Its finite volume solver for the steady/unsteady, compressible/incompressible Navier-Stokes equations can be applied to a large range of vehicle geometry and speed regimes. Multiple turbulence models are available as well as large-eddy simulation capabilities including hybrid RANS/LES models. The approach used for this HL-CRM analysis includes the use of low-Mach pre-conditioning, the one-equation Spalart-Allmaras turbulence model with rotation and curvature corrections (SARC) and the Quadratic Constitutive Relation (QCR) turned-on with the CR1 coefficient set to 0.35. These particular solver settings are aligned with the OVERFLOW setup described next.

The OVERFLOW flow solver, version 2.2g, is a node-based RANS code specifically designed for structured, overset grid systems. A list of solver options exercised for the HL-CRM analysis is provided below.

- HLLE++ upwind flux method
- SSOR implicit solver
- TLNS3D dissipation scheme
- van Albada limiter
- low Mach pre-conditioning off
- 3rd order spatial accuracy
- global multi-grid off
- DT = 0.1, CFLMIN = 5.0
- Spalart-Allmaras turbulence model with rotation and curvature corrections (SA-noft2-RC)
- Quadratic Constitutive Relation (QCR), CNL1 = 0.35

All cases were run with the assumption of fully developed boundary layers (i.e., without laminar/turbulent transition modeling). For computations for flight conditions, the Reynolds number was 24.6 million, corresponding to a freestream Mach number of 0.2 at an altitude of 10,000 ft. For computations at wind-tunnel conditions, the Reynolds number was set at 3.3 million based on an assumed model scale of 10%, sea-level conditions, and a freestream Mach number of 0.2.

The geometric parameters used for computing all force and moment coefficients are summarized as follows:

C_{ref} = 275.8 in (MAC)
$S_{ref}/2$ = 297,360.0 in^2
b/2 = 1156.75 in
X_{ref} = 1325.9 in, Y_{ref} = 0.0 in, Z_{ref} = 177.95 in

3.3 CFD Results for Conventional HL-CRM Configuration

The nominal slat and flap deflections were analyzed for both takeoff and landing cases using CFD++ and OVERFLOW. The nominal takeoff slat and flap deflection is 22° and 25°, respectively. The corresponding landing deflections are 30º and 37º.

Comparisons of computed lift and pitching moment are provided in Figure 11 where the CFD++ results are plotted as blue, solid lines and the OVERFLOW predictions as red, dashed lines. Takeoff results have a square symbol and landing a triangle. The takeoff results for both codes are in good agreement up to an angle-of-attack of 14º. Between 14º and 17º, the methods differ on stall prediction with CFD++ showing a break in the lift curve at 16º while OVERFLOW data breaks at 17º. Discrepancies at or near stall are expected as modeling the complex flow physics of a high-lift system at high angles-of-attack is known to push the limits of RANS methods where variables such as mesh density and turbulence modeling can be strong drivers for the solution. A similar comparison is shown for the landing configuration but with more discrepancy through the linear portion of the lift curve where OVERFLOW predicts roughly 0.05 higher C_L. Overall, the code-to-code lift comparison is reasonable and offers some reassurance that the high-lift design is operating at representative levels with landing C_{Lmax} in the neighborhood of 2.3 to 2.4.

The predicted pitching moment curves in Figure 11 show that CFD++ results are more nose-down for takeoff and more nose-up for landing compared to OVERFLOW at a given lift level. While the more nose down results for OVERFLOW at landing could likely be explained by more effective flaps relative to CFD++ (which would also explain the improved lift), no explanation has yet been found for the takeoff differences. Both methods show a strong nose-down pitch break at stall, which is a good indicator of a representative design.

Upper surface streamlines and skin friction contours are provided in Figures 12 and 13 to show where flow separation initiates for the takeoff and landing configurations. Both CFD++ and OVERFLOW predict the same flow mechanism limiting C_{Lmax}: large-scale separation directly behind the nacelle. Note that the geometries analyzed do not include a nacelle chine often used to control the separation pattern behind the nacelle.

3.4 CFD Results for Simplified HL-CRM Configuration

Nominal slat (25°) and flap deflections (50°) were analyzed for landing cases using CFD++. Upper surface streamlines and skin friction contours are provided in Figure 14 to show where flow separation initiates in the absence of AFC. For reference, OVERFLOW solutions for the conventional HL-CRM concept in landing-approach configuration are provided as well. As was expected, the simplified HL-CRM exhibits fully separated trailing edge flaps whereas the conventional HL-CRM concept features mostly attached flow over the slotted trailing edge flaps. Separated flow over the simply hinged flaps of the simplified HL-CRM makes them much less effective than their slotted counterparts on the conventional HL-CRM, producing reduced lift as shown in the comparisons of computed lift variations with angle of attack in Figure 15 for both simplified and conventional HL-CRM concepts. Computed lift also indicates that while the conventional HL-CRM produces higher C_{Lmax}, it also stalls sooner. Recalling that the slat settings are the same for both the conventional and the simplified HL-CRM concept, one could say that the simplified HL-CRM is in a sense overprotected against stall by the slat since its wing is less loaded due trailing edge flap separation across all angles of attack. This interpretation carries over to a comparison of computed pitching moment for the two HL-CRM concepts. Whereas the

conventional HL-CRM exhibits the desired post-stall nose-down pitching moment, the pitching moment for the simplified HL-CRM concept seems to indicate incipient stall.

Note that the difference in predicted lift for the conventional and simplified HL-CRM concepts also quantifies the decrements in high-lift performance for the simplified high-lift system that need to be recovered by the integration of AFC.

4.0 AFC SIZING FOR HIGH LIFT APPLICATIONS

While AFC was demonstrated as an effective means for recovering aerodynamic performance for the CRM concept with a mechanically simplified high-lift system in the predecessor to the current study, the power requirements of this initial AFC high lift application were prohibitive for any feasible system integration solutions with realistic transonic transport aircraft concepts [5]. The excessive AFC power requirements observed for the initial AFC implementation motivated the current study in order to provide guidance for devising more practical AFC-enhanced high-lift systems.

4.1 Fluidic Oscillators

In the initial pilot study [5], the AFC implementation utilized a total of 74 convergent/divergent nozzle elements placed into both inboard and outboard trailing edge flaps on a HL-CRM concept. The power requirements for these AFC nozzle arrays called for 72 lbs/sec air mass flow at an operating pressure of 80 psia. To put this in perspective, 1990s-era jet engines can provide about 8 lbs/sec air mass flow at that operating pressure.

These AFC power requirements were correlated with measured mass flow requirements for an AFC application to the vertical tail of a B757 aircraft [3]. While comparable to these measured mass flow rates, accounting for scaling effects, it looked like the realized mass flow rates on this large-scale AFC integration were somewhat lower than the AFC for high-lift power requirements.

To better understand the effect of the type of AFC implementation, the convergent/divergent AFC nozzles in the high-lift application were substituted with fluidic oscillators. Figure 16 shows the integration of both nozzles and fluidic oscillators in the inboard and outboard trailing edge flaps of the simplified CRM. Note, that this version of the simplified high-lift CRM is different from the one presented in the current report. This earlier version used drooped leading edges rather than slats, and the trailing edge flaps were deflected at 30° rather than at 50° as shown in Figure 6. This earlier simplified HL-CRM variant will be referred here as SHL-CRM.v1.

Figure 17 shows computed surface pressures for the SHL-CRM.v1 concept with either constant blowing through ducts or sweeping jets expelled through the fluidic oscillators. The gray surfaces designate pockets of separated flow. This figure suggests that both AFC high-lift applications are about equally effective.

Figure 18 shows the AFC mass flow rates required to have the simplified match the lift generated by the conventional HL-CRM.v1 concept at a nominal operating landing-approach operating condition. The AFC implementation using fluidic oscillators indeed require about 5% less mass flow than the duct AFC installation at a still high operating pressure of about 80 psia. These results indicate that the fluidic oscillators offer modest reductions in mass flow rates relative to steady blowing.

4.2 Reynolds Number Effects

It is well understood that flow viscosity affects the aerodynamic performance of high-lift systems. Generally speaking, lift measured or computed at wind-tunnel (i.e., model scale) conditions is lower than at flight conditions (i.e., full scale) due to the de-cambering effect of the thicker boundary-layer flow at wind-tunnel conditions associated with lower Reynolds numbers. As the AFC high-lift feasibility study on SHL-CRM.v1 was conducted at wind-tunnel conditions (with a view toward experimental verification), the question is whether the AFC power requirements could be reduced by deploying AFC to reattach the thinner boundary layer flow at flight conditions rather than the thicker (lower Reynolds number) boundary layer flow at wind-tunnel conditions.

Figure 19 shows lift curves computed from RANS solutions for the conventional and simplified HL-CRM.v1 concepts. The lift-reducing effects due to a lower Reynolds number are noticeable for both variants of the HL-CRM.v1 concept. The two red-colored symbols indicate the lift produced by the AFC-enhanced simplified HL-CRM.v1 concept at a nominal landing approach flight condition. Note that both AFC applications use the same normalized mass flow rate to recover the lift produced by the conventional HL-CRM.v1 concept at both wind-tunnel and flight Reynolds number. Thus, Reynolds number effects also play a secondary role in driving the power requirements for AFC high lift applications.

4.3 Trailing Edge Flap Geometry Effects

The simply hinged flap on the simplified HL-CRM.v1 concept was sized to match the size and deflection of the slotted trailing edge flap of the conventional HL-CRM.v1.

To develop an idea about effect of flap size and deflection on the aerodynamic performance of a simplified HL-CRM.v1 concept, linear potential solutions were computed for inviscid flow over the simplified HL-CRM.v1 concept for two flap chord sizes (18% and 22.5% mean aerodynamic chord) and for two flap deflection angles (30° and 50°). Solutions for inviscid flow solutions help address the affects of flap geometry on ideal high-lift characteristics and avoid having the answers clouded by issues related to Reynolds-number dependent separated flow.

Figure 20 shows the surface pressures computed from linear potential flow solutions for four trailing-edge flap geometry/deflection combinations. These results show that the flap chord size has a relatively small effect on the wing pressure distribution, and thereby, lift. However, increasing the flap deflection from 30° to 50° noticeably reduces the upper wing pressures, particularly along the wing leading edge and the flap hinge lines and thereby increasing lift. This has led to the selection of the original flap chord 50° down deflection as the revised configuration for the subsequent studies.

4.4 AFC Actuator Sizing and Placement

This aspect of the AFC design trade study aimed at providing sensitivities for chordwise placement of AFC actuators, for alignment requirements of AFC jets with wing surface flow, and for mass flow rate selection. For quick turnaround, these sensitivity studies were conducted for two-dimensional flow over airfoils. Figure 21 illustrates that two-dimensional flow analyses can be expected to provide meaningful insights. This figure shows surface pressures wing and surface stream lines computed from RANS solutions for the simplified HL-CRM.v1. These images show little wing surface cross flow.

The two-dimensional airfoil geometry used in the present sensitivity studies were defined by wing cuts at the mid flap butt station, for both the inboard and the outboard simply hinged trailing edge flaps.

Figure 22 summarizes the results from these parametric AFC jet placement and sizing studies. Results are shown for the mid inboard flap configuration; they are very similar to the results obtained for the mid outboard flap configuration. The key takeaways from these results are: (1) shallow AFC jet angles correspond to alignment with the local surface flow, and the better this alignment is, the more effective AFC is; and (2) AFC placement close to the separation point improves flow control effectiveness.

Figure 23 shows an initial application of the findings from this sensitivity study to the simplified HL-CRM.v1 concept. Here, AFC is applied as a surface boundary condition in spanwise segments on the inboard flap only. The segmentation allows for a closer alignment of the AFC jets with the local surface flow along the trailing edge flap hinge line. The computed surface pressures and the envelopes over regions of separated flow indicate the effectiveness of AFC for suppressing flow separation over the inboard trailing edge flap. Plotting lift as a function of AFC mass flow rate, shows that the current AFC application recovers the lift of the conventional HL-CRM.v1 concept at about half the mass flow required in the AFC application in the pilot study reported in Reference 5.

Additional parametric AFC implementation studies explored the affect of lateral AFC jet angles (i.e., directing AFC jets +/-11° out of the freestream plane) of using AFC for reducing the vertical flow alongside the flap side edges. None of these parametric variations produce discernible improvements over the AFC application summarized in Figure 23.

4.5 AFC Actuation – Discrete Ducts

Figure 24 summarizes the findings for AFC application to the simplified HL-CRM.v1 concept using constant blowing through discrete ducts. There are either 20 or 40 ducts placed into the inboard trailing edge flap. The exit area of the AFC actuators is of the same size (0.5” wide by 0.25” tall) as in the B757 AFC application in Reference 3. Looking at the variations of lift with the mass flow rate and the number of AFC units, it is concluded that AFC effectiveness is primarily driven in this AFC implementation by the total AFC mass flow rate. Put another way, to achieve the same AFC effectiveness with half the number of AFC actuators, one has roughly to double the operating pressure.

Compared to the AFC mass flow rates shown in Figure 23, they were reduced by half by going from the AFC simulation through boundary conditions to the actual modeling of the individual AFC actuators. Also, the AFC mass flow rates in Figure 24 are roughly a quarter of the required AFC mass flow rate of 36 lbs/sec per half wing in the initial AFC application in the prior AFC high lift study in Reference 5.

4.6 AFC Actuation – Continuous Spanwise Slot

The results in Figure 24 suggest that the number of actuators can be traded against operational pressure for any given mass flow rate. As mentioned, the original AFC high-lift implementation in Reference 5 proved infeasible because it required a mass flow rate at an operational pressure that exceeded typical engine core bleed capabilities. However, system trade studies in Reference 5 also hinted that AFC for high-lift could become feasible if the operating pressure

could be lowered because the stumbling block was not so much the air mass flow rate by itself but that AFC mass flow rate at high operating pressures.

This suggested a preference for AFC implementations with more AFC units and lower operating pressures. Taken to the extreme, that suggests exploring the option of using a duct that runs the full span of the inboard trailing edge flap.

This concept of such spanwise continuous slot and its results are illustrated in Figure 25. This composite figure shows the implementation of the AFC duct concept. The visualizations of computed RANS solutions for their operating pressures show that AFC if effective in maintaining attached flow over the trailing edge flap for operating pressure ratios around 2 (i.e., about 60 psia). As the computed variations of lift with AFC mass flow indicate, there appears to be a compounding effect by going from discrete AFC units to the spanwise continuous slot concept. While this still needs to be better understood, it can be surmised that this benefit is associate with the avoidance of total pressure losses associated with the internal-corner flows of the discrete AFC units.

4.7 Traversing AFC Actuation

Here, the traverse actuation [11, 12] is employed, which is currently developed by Boeing for reduced mass-flow requirement compared to a steady-state actuation. This concept is illustrated in Figure 26, whereby a small and fast moving jet packet travels periodically in the span wise direction, much like a crabwise motion. There, a quarter or an eighth of the spanwise continuous slot is actuated as shown in the middle and right hand side flow fields, respectively. The high momentum jet packets move inboard at a frequency of either 10 Hz or 100Hz. The 10Hz actuation is consistent with characteristic length and time scales of the overall wing flow. It results in favorable coupling between the flow control excitation and the surrounding flow, with commensurate mass flow reduction, between 3 lbs/sec and 4 lbs/sec at an operating pressure ratio of 2.4.

The lift versus angle-of-attack plot in Figure 27 summaries the results for applying the best performing high-lift AFC implementation – based on the current parametric design and sensitivity studies – to the simplified HL-CRM concept introduced in this report. All solutions in this plot were computed from OVERFLOW RANS solutions for a flight Reynolds number of 24.6 million. The black solid line and the dashed blue lines give the lift for the conventional and the simplified HL-CRM wing/body/nacelle/pylon concept, respectively. The lift given by the green dashed line is computed using steady blowing (mass flow rate about 10.2 lbs/sec) through a spanwise continuous slot running the span of the inboard simply hinged trailing edge flap. The red diamond symbol shows the application of the best-in-class traverse AFC actuation at and angle of attack of 8°. This angle of attack is chosen because it corresponds to a nominal landing approach flight condition for the reference conventional HL-CRM concept. This figure illustrates that the current AFC high-lift application succeeds in recovering most of the aerodynamic performance losses one encounters by going from a conventional to a simplified HL-CRM configuration.

Note that the AFC high-lift application reported in Figure 27 is based on parametric studies for an earlier design iteration on the HL-CRM concept. Repeating these design and sensitivity studies for the current simplified HL-CRM release can be expected to refine the current high-lift

AFC application, as will further tuning of the traversing AFC actuation (e.g., multiple traversing AFC jet packs as opposed to the single packet actuation).

5.0 TRADE STUDY ON AFC-ENABLED SIMPLIFIED HIGH-LIFT SYSTEM

This section discusses results from a system-level trade study on the mechanically simplified high-lift system to accommodate a pneumatic AFC system defined and sized in the preceding section. The purpose of this trade study is to identify any potential weight and fuel savings from the mechanically simplified high-lift system. This requires a baseline transonic transport concept configuration to increment any such potential savings from. In this study, the NASA ERA-0003 concept was chosen to be that baseline concept. The ERA-0003 concept represents a twin-aisle 275-passenger transonic transport aircraft with 1990-era technology projections [13]. Its high lift system was comprised of Krueger flaps and of single-element slotted trailing edge flaps. These features make the ERA-0003 concept comparable to one that the CRM OML was defined for. Key dimensions for the ERA-0003 concept are provided along with a 3-view and a cabin layout in Figure 28.

It is assumed that the auxiliary power unit (APU) can provide pressurized air mass flow rate of 8 lbm/sec at an operating pressure of 60 psia for the AFC-enhanced high lift system. Initially, it was assumed that AFC would reduce operational empty weight (OEW) as it enables a mechanically much simpler and thus lighter high-lift system. A mass properties build-up showed that any of these weight reduction benefits are likely negated by the weight additions due to AFC redundancies for flight safety. For instance, while there are already pneumatic lines connecting the APU in the empennage of the airplane with the main engines (used for powering up), these lines are not flight critical. Now that they are also used for feeding the AFC high-lift system, they need to be fortified or redundant plumbing needs to be installed. In view of this, going from a conventional to an AFC-enhanced high-lift system was treated as weight neutral for the current system performance trade studies.

Substituting simply-hinged trailing edge flaps for the ERA-0003 slotted trailing edge flaps with Fowler allows elimination of the flap fairings. This reduces cruise drag by 1.65 counts of excrescence drag per external fairing pair. This assumes that there are two exposed fairings for the inboard flap, whereas current design practice calls for one outboard external fairing and the inboard flap mechanism embedded in the side of fuselage.

Figure 29 summarizes the mission performance for the ERA-0003 baseline configuration (far left column), for an unscaled, and for two resized AFC-variants of the ERA-0003 (two right-most columns in Figure 29). The unscaled AFC variant looks in all aspects just like the baseline ERA-0003 except for the no longer required high-lift system fairings for both inboard and outboard simply hinged trailing edge flaps. Elimination of these fairings reduces cruise drag by 3.3 counts. It is still assumed that 2% engine core bleed is needed to power the AFC high-lift system due to line losses for the APU supplied air mass flow. As that core bleed required to feed the AFC system reduces maximum available engine thrust, TOFL increases by about 194 ft. The unscaled AFC variant of the ERA-0003 concept also shows a 1.46% gain in range compared to the baseline ERA-0003 design because of the reduced cruise drag.

One of the two resized AFC variants of the ERA-0003 increases engine size to compensate for the core bleed such that the original takeoff distance of 8,668 ft is met. The other resized AFC variant of the ERA-0003 trades wing area and engine size such that it minimizes fuel burn

while meeting all design requirements and constraints. These resized AFC variants for the ERA-0003 concept aircraft yield savings in fuel burn of 1.94% and 2.25%, respectively.

These results are illustrated in the 'thumbprints' in Figures 30 and 31. These plots show lines of constant TOGW, block fuel, rejection field length, optimum altitude, and distance to climb, all plotted against engine thrust (vertical axis) and wing area (horizontal axis). For the baseline ERA-0003 concept in Figure 30, the mission calls for a climb in 200 nm to an initial cruise altitude (ICA) of 35,000 ft. The point where the lowest possible constant fuel burn trace touches the climb-to-ICA boundary sizes the ERA-0003 concept. Figure 31 illustrates the performance of the three AFC variants of the ERA-0003 concept. The unsized AFC variant violates the takeoff distance constraint. The AFC variant with the resized engine recovers the takeoff distance constraint by compensating for the 2% engine core bleed that is required to supplement the AFC power requirements. Finally, the AFC variant that trades both wing area and engine thrust is sized by the lowest possible fuel burn that still permits to meet both takeoff distance and climb distance to initial cruise altitude.

5.1 Net Present Value (NPV) Assessment

The NPV assessment is carried out for the best–in-class AFC variant of the ERA-0003 concept. Flying the same mission as the baseline ERA-0003 concept, its AFC variant is estimated to save 5,135 lbs or about 790 gals of jet fuel per flight. Assuming average flight duration of 16 hours per trip and major maintenance intervals of 10,000 flight hours, there are 625 flights between major maintenance stand downs. With 10 major maintenance cycle during an assumed 20-year operational life, the aircraft will complete about 6,000 flights in its lifetime or 300 flights for every year of operation. This translates to lifetime fuel savings of about 4.74 million gallons of fuel.

The amount of cost savings over the lifetime of an AFC-enabled ERA-000-type aircraft depends on assumptions of fuel price and of a discount rate. The discount rate is a function of the weighted average cost of capital (WACC) of the operator of such an aircraft. The latter directly depends on the capital structure of the operator and its credit rating, and indirectly on macroeconomic factors such as market interest and inflation rates. For the sake of producing an NPV dollar estimate, let the fuel price be assumed at $2/gal on average for the 20-year operational flight, and a discount rate of 10%. This would translate into an NPV of $9.48M per AFC-variant of an ERA-0003-like concept over its 20-year operational life. While this dollar amount might be subject to debate due to the assumption about future fuel prices and operator WACC, the key takeaway here is that the NPV is positive, indicating that there might be value in considering AFC-enabled mechanically simpler high-lift system for an ERA-0003-class aircraft.

6.0 ANALYSIS, CONCLUSIONS, AND RECOMMENDATIONS

The key findings of the current trade study on AFC-enhanced mechanically simplified high-lift systems for commercial transports indicate platform performance improvements due to OEW savings (primarily due to the elimination of the mechanical systems facilitating the Fowler motion of the trailing-edge slotted flaps) and improved aerodynamics (i.e., elimination of high-lift systems fairings). These platform performance improvements translate into a positive NPV, indicating value to an operator to acquire such AFC-enhanced transport aircraft, although the actual NPV amount might be subject to debate.

These key findings hinge on the assumption that further AFC integration studies will identify options for fully recovering the aerodynamic high-lift performance of a baseline concept (e.g., the ERA-0003 or the HL-CRM). Current AFC implementation on a simplified HL-CRM concept indicates a shortfall in recovering the high-lift performance of the conventional HL-CRM concept.

Several potential options have been identified for further improving the effectiveness of AFC-enhanced high list systems. Among them are better sensitivities for an optimal deflection of the simply hinged trailing edge flaps and further refinement of the implementation of the traversing AFC concept.

In all these AFC high-lift system integration studies, the focus has been on matching the landing-approach performance of a conventional high-lift CRM concept. This has been considered the most demanding benchmark for an AFC-enhanced high lift system as it must achieve maximum aerodynamic performance with minimum power requirements as the jet engines as main onboard power sources run in almost idle. Now that it seems a path has been identified to take that hurdle, the AFC-enhanced high-lift system needs to be refined to work for both takeoff and landing approach over a range of operational conditions. For instance, retracting the current simply hinged flaps from a landing approach to a takeoff setting would cause the spoiler to cover up the spanwise continuous slot needed for the otherwise promising traversing AFC actuation. Technical solutions could involve multiple or staggered AFC ducts, or AFC-in-wing versus the current AFC-in-flap design solutions.

These technology maturation efforts are expected to benefit from a wind-tunnel test program to calibrate if not validate the CFD-based analysis and design tools. While computer aided definition (CAD) models for the outer mold lines (OMLs) of a conventional and simplified HL-CRM concept have been made available as part of this study, along with detailed guidance as to rigging of the high-lift surfaces and flap fairings, further refinements to these definitions are expected once the development of wind-tunnel model design requirements has commenced in earnest.

7.0 REFERENCES

[1] McLean, J.D., Crouch, J.D., Stoner, R.C., Sakarai, S., Seidel, G.E., Feifel, W.M., and Rush, H.M., “Study of the Application of Separation Control by Unsteady Excitation to Civil Transport Aircraft, NASA Contractor Report, NASA-CR-1999-209338, June 1999.

[2] DeSalve, M., Whalen, E., and Glezer, A., ” High-Lift Enhancement Using Active Flow Control,” AIAA Paper 2012-3245, June 2012.

[3] Whalen, E.A., Lacy, D.S., Lin, J.C., Andino, M.Y., Washburn, A.E., Graff, E.C., and Wygnanski, I.J., “Performance Enhancements of a Full-Scale Vertical Tail Model Equipped with Active Flow Control,” AIAA Paper 2015-0784, January 2015.

[4] Lin, J.C., Whalen, E.A., Eppink, J.L., Siochi, E.J., Alexander, M.G., and Andino, M.Y., “Innovative Flow Control Concepts for Drag Reduction,” AIAA Paper 2016-0864, January 2016.

[5] Hartwich, P.M., Dickey, E.D., Sclafani, A.J., Camacho, P.P., Gonzales, A.B., Lawson, E.L., Mairs, R.Y., and Shmilovich, A., “AFC-Enabled Simplified High-Lift System Integration Study,” NASA CR 2014-218521, September 2014.

[6] Lacy, D.S., and Sclafani, A.J., "Development of the High Lift Common Research Model (HL-CRM): A Representative High Lift Configuration for Transonic Transports, AIAA Paper 2016-0308, January 2016.

[7] Vassberg, J.C., DeHaan, M.A., Rivers, S.M., Wahls, R.A., "Development of a Common Research Model for Applied CFD validation," AIAA Paper 2008-6919, August 2008.

[8] NASA Common Research Model , URL: http://commonresearchmodel.larc.nasa.gov, February 2008.

[9] Sclafani, A. J., Slotnick, J. P., Vassberg, J. C., Pulliam, T. H., Lee, H. C., "OVERFLOW Analysis of the NASA Trap Wing Model from the First High Lift Prediction Workshop," AIAA Paper 2011-0866, January 2011.

[10] Sclafani, A. J., Slotnick, J. P., Vassberg, J. C., Pulliam, T. H., "Extended OVERFLOW Analysis of the NASA Trap Wing Wind Tunnel Model," AIAA Paper 2012-2919, June 2012.

[11] Shmilovich, A., Yadlin, Y. and Clark, R.W., "Traversing Jet Actuator", US Patent 8,336,828, December, 2012.

[12] Shmilovich, A. and Yadlin, Y., "Method and Apparatus for Supplying a Gas Jet Over an Aerodynamic Structure", US Patent 8,827,212, September, 2014

[13] Bonet, J. T., Schellenger, H. G., Rawdon, B. K., Elmer, K. R., Wakayama, S. R., Brown, D., and Guo, Y. P., "Environmentally Responsible Aviation (ERA) Project – N+2 Advanced Vehicle Concepts Study and Conceptual Design of Subscale Test Vehicle (STV)," NASA Contract Report 2013-216519, 2013.

8.0 FIGURES

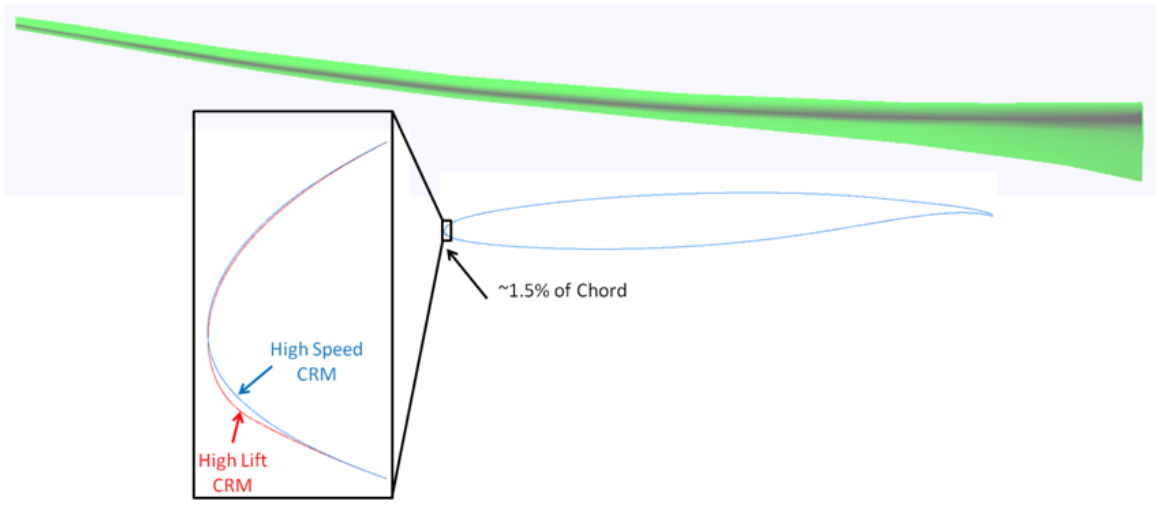

Figure 1 Front view of High Speed CRM wing showing bending, and an example of leading edge curvature modification to high speed CRM wing sections to make it more amenable to low-speed operation.

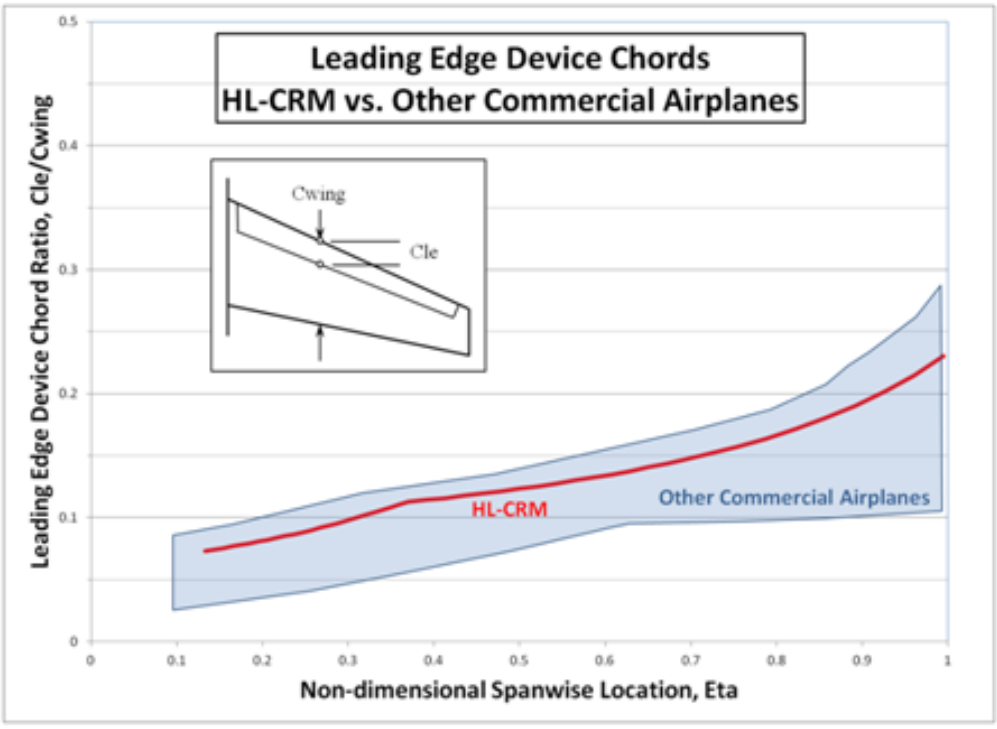

Figure 2 Non-dimensional HL-CRM leading edge chord distribution relative to other commercial airplanes.

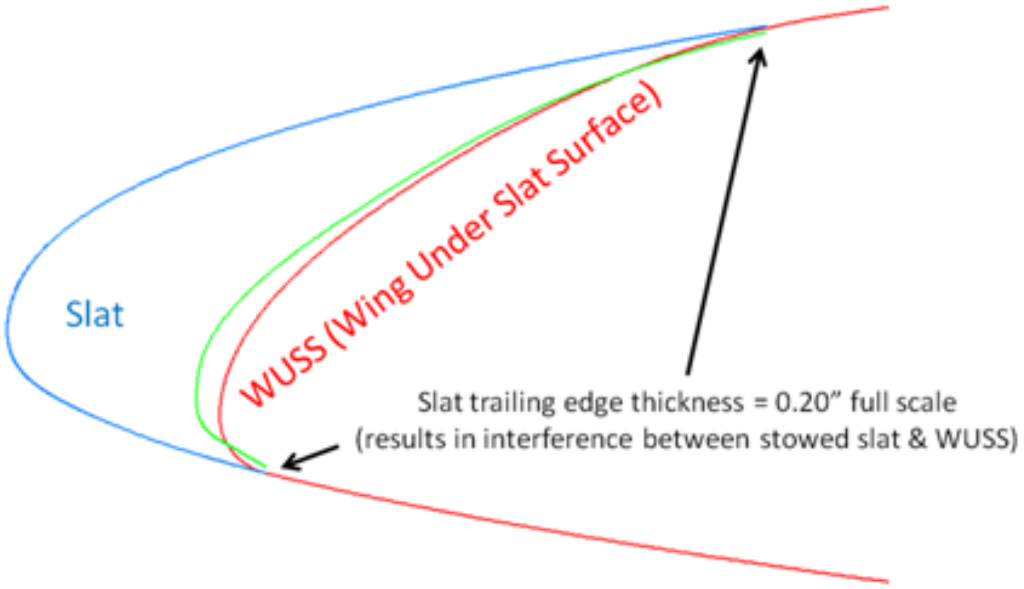

Figure 3 Cross section of outboard slat and WUSS.

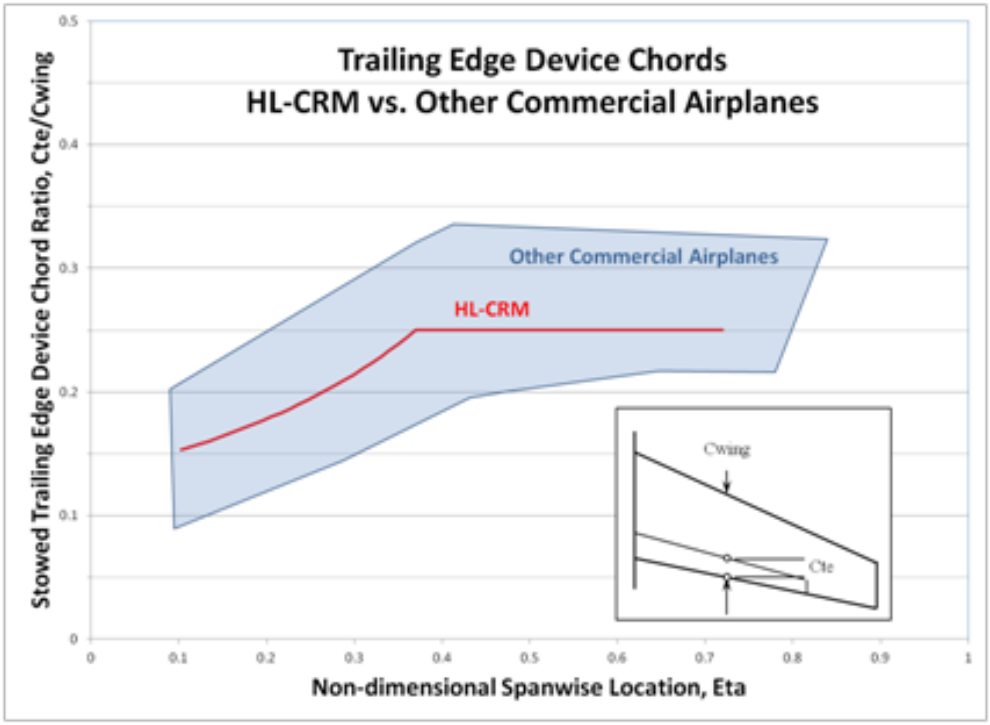

Figure 4 Non-dimensional HL-CRM leading edge chords relative to other commercial airplanes.

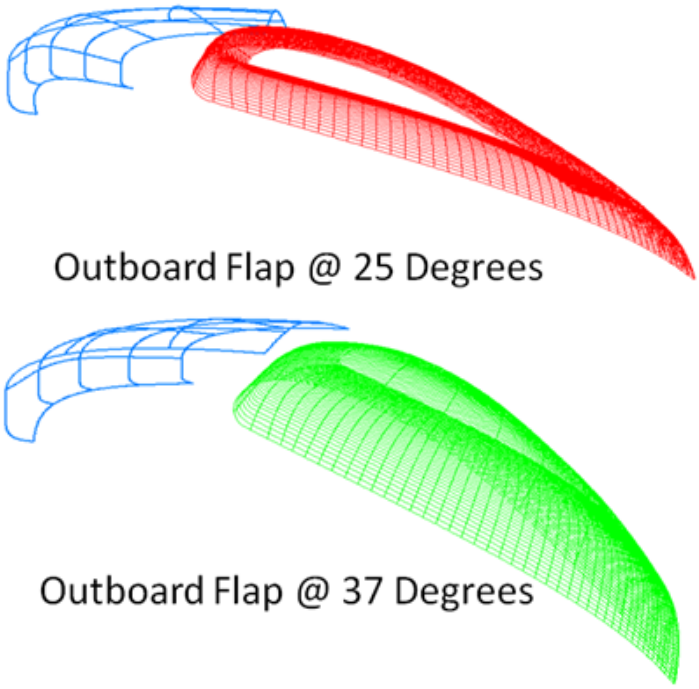

Figure 5 Positioned outboard flaps illustrate how the flap leading edge tracks the spoiler trailing edge to provide uniform gap distribu-

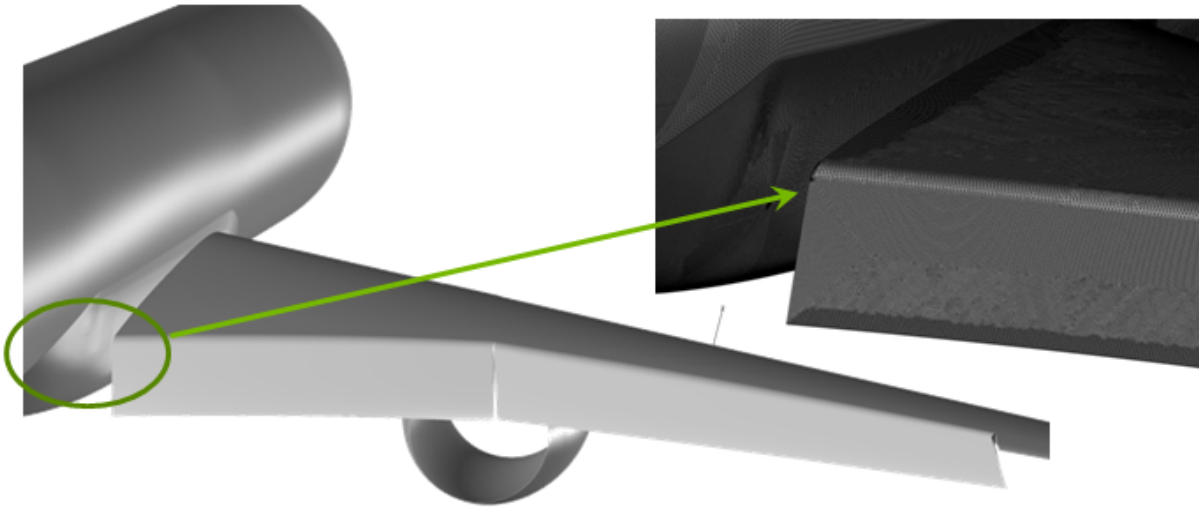

Figure 6 Illustration of simplified HL-CRM concept with simply hinged trailing edge flap deflected by 50°.

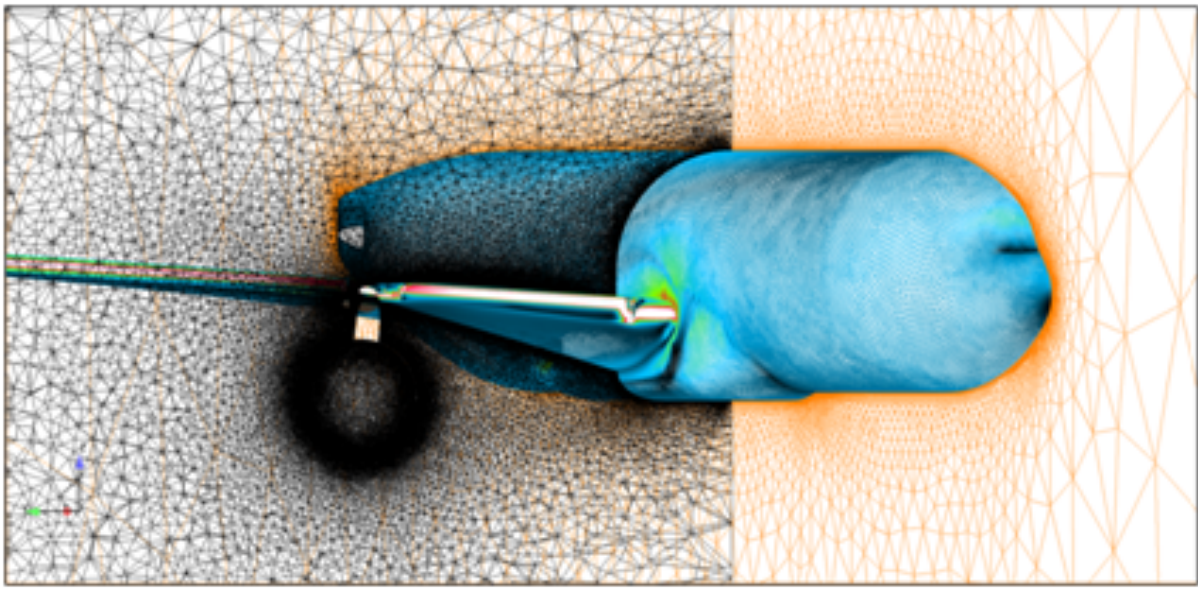

Figure 7 Anisotropic tetrahedral mesh of HL-CRM in takeoff configuration for CFD++ flowfield computations.

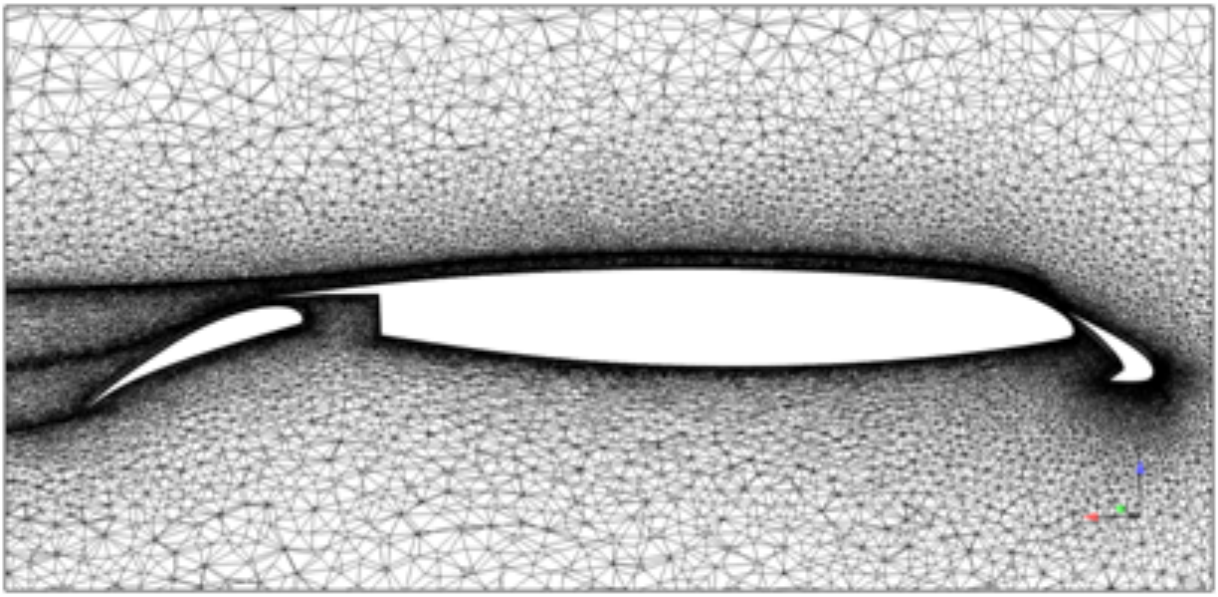

Figure 8 Anisotropic tetrahedral mesh at a wing butt station for HL-CRM in takeoff setting illustrates resolution of viscous wakes of wing and high-lift elements

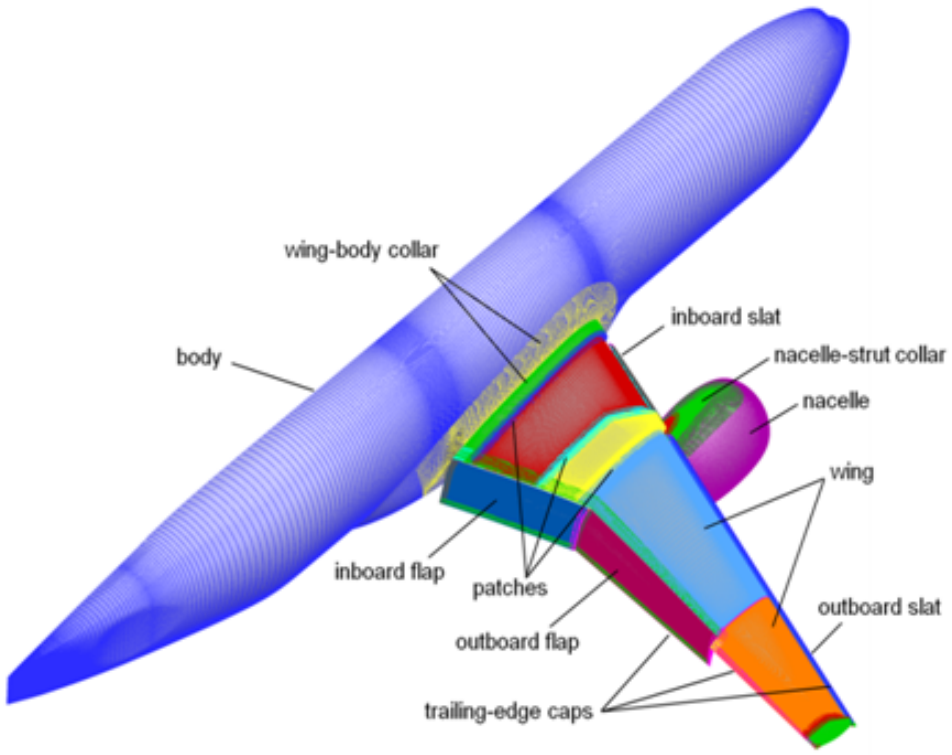

Figure 9 OVERFLOW surface grid topology.

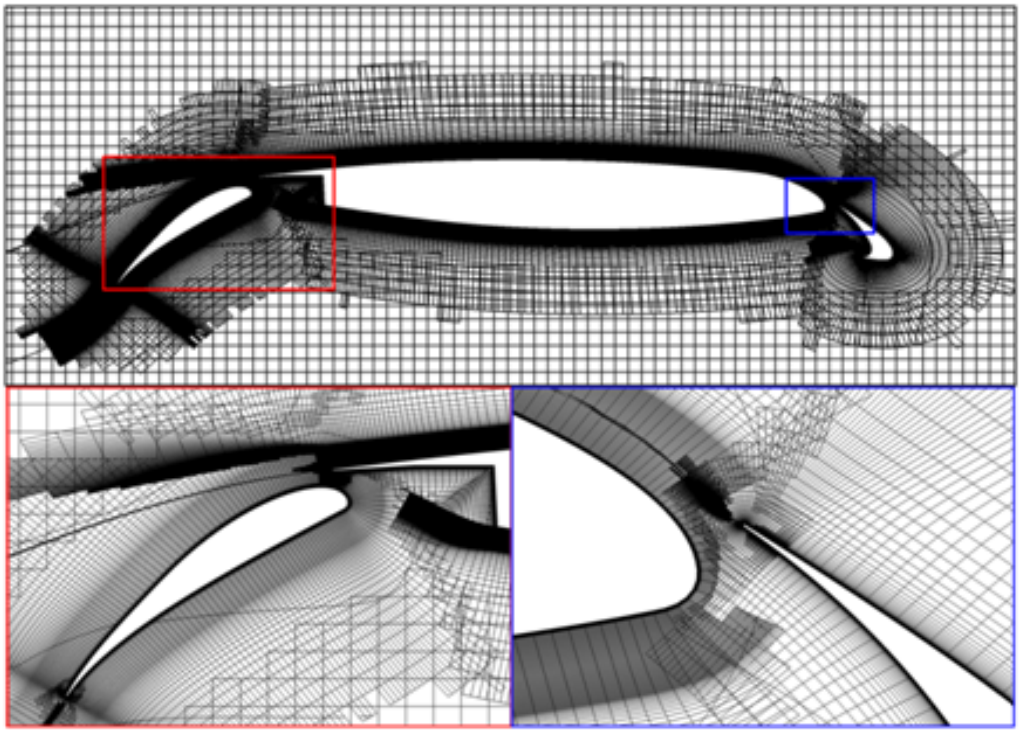

Figure 10 OVERFLOW volume grid - mid-span wing slice.

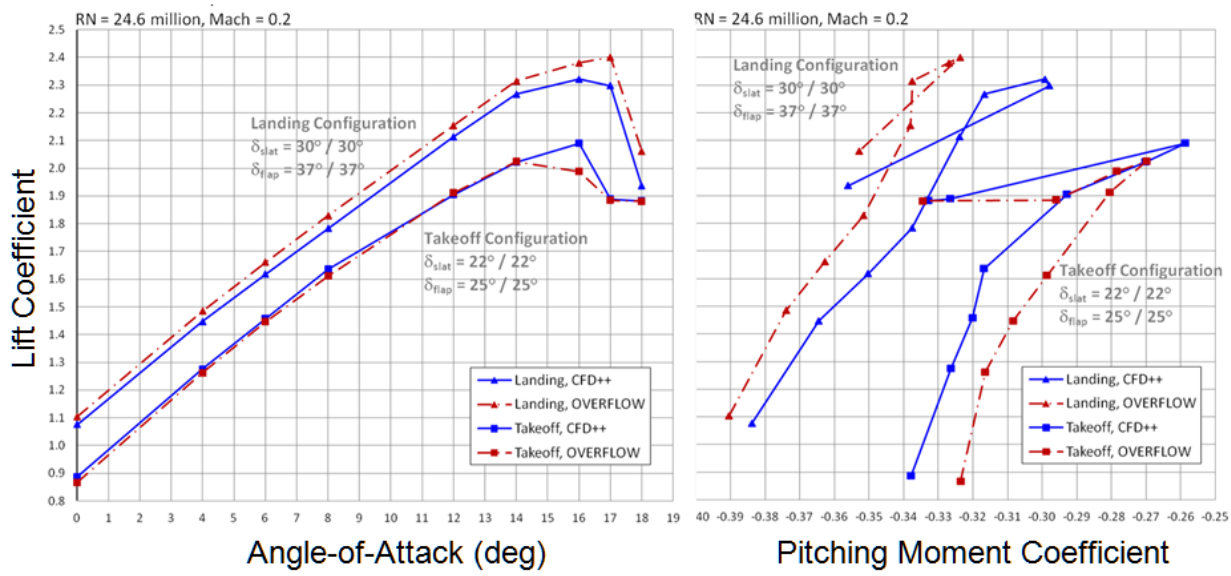

Figure 11 Lift and pitching moment curves as computed with CFD++ and OVERFLOW for the conventional HL-CRM concept in takeoff and landing-approach configuration.

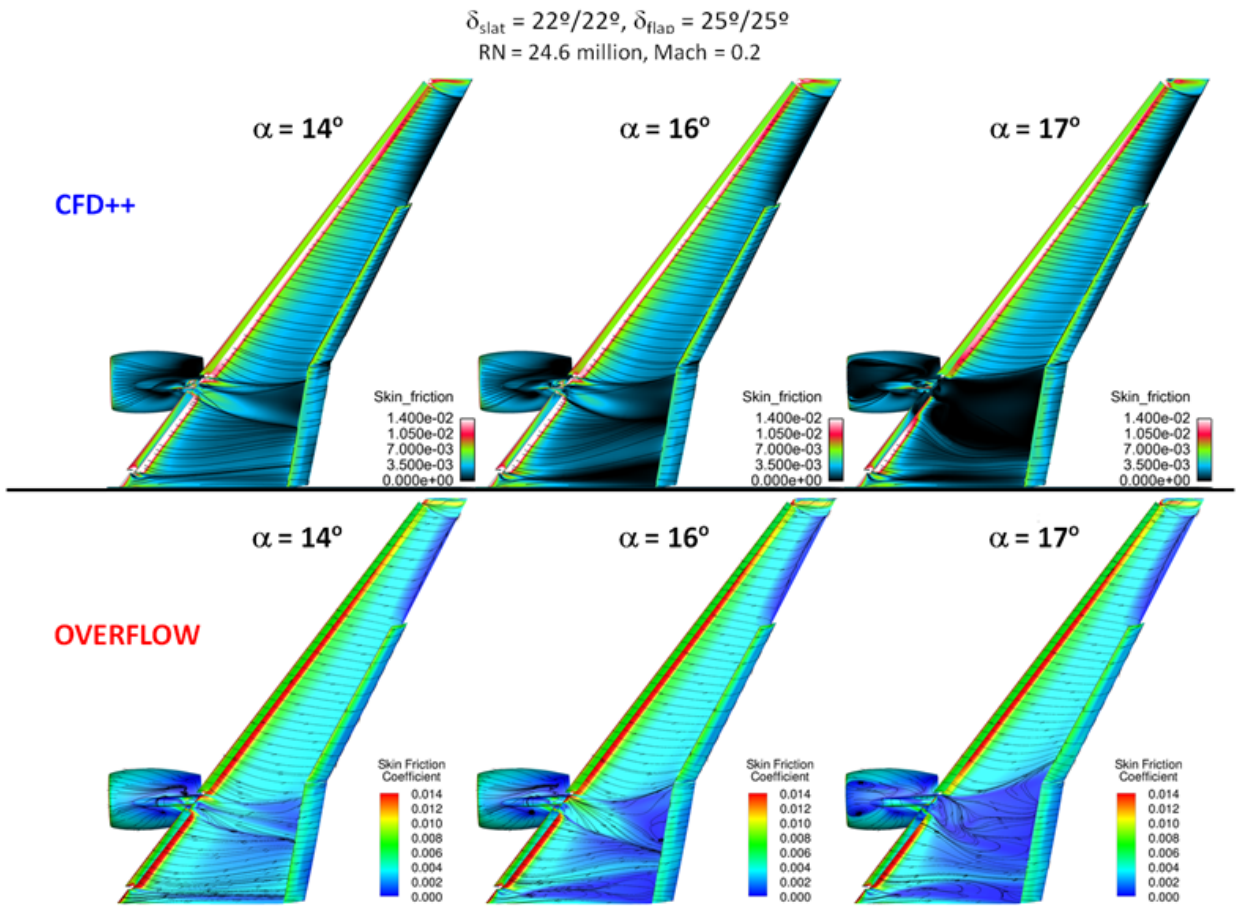

Figure 12 Surface streamlines and skin friction distribution for HL-CRM in take off configuration.

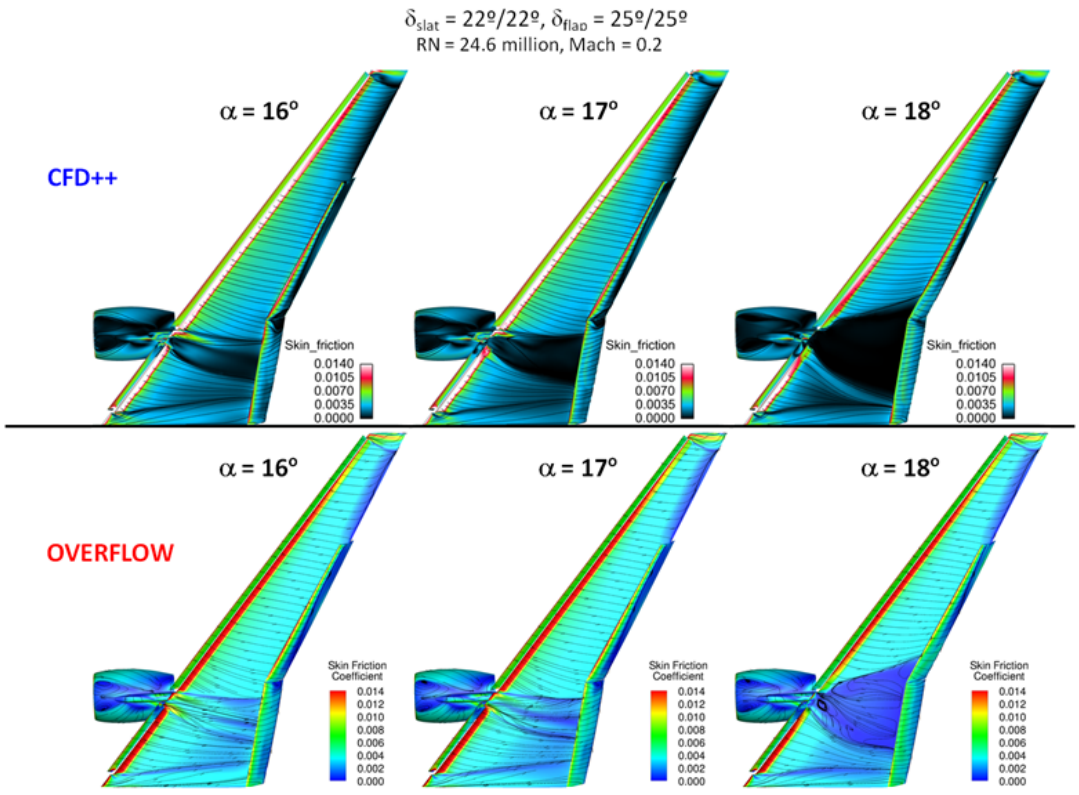

Figure 13 Surface streamlines and skin friction distribution for HL-CRM in landing-approach configuration.

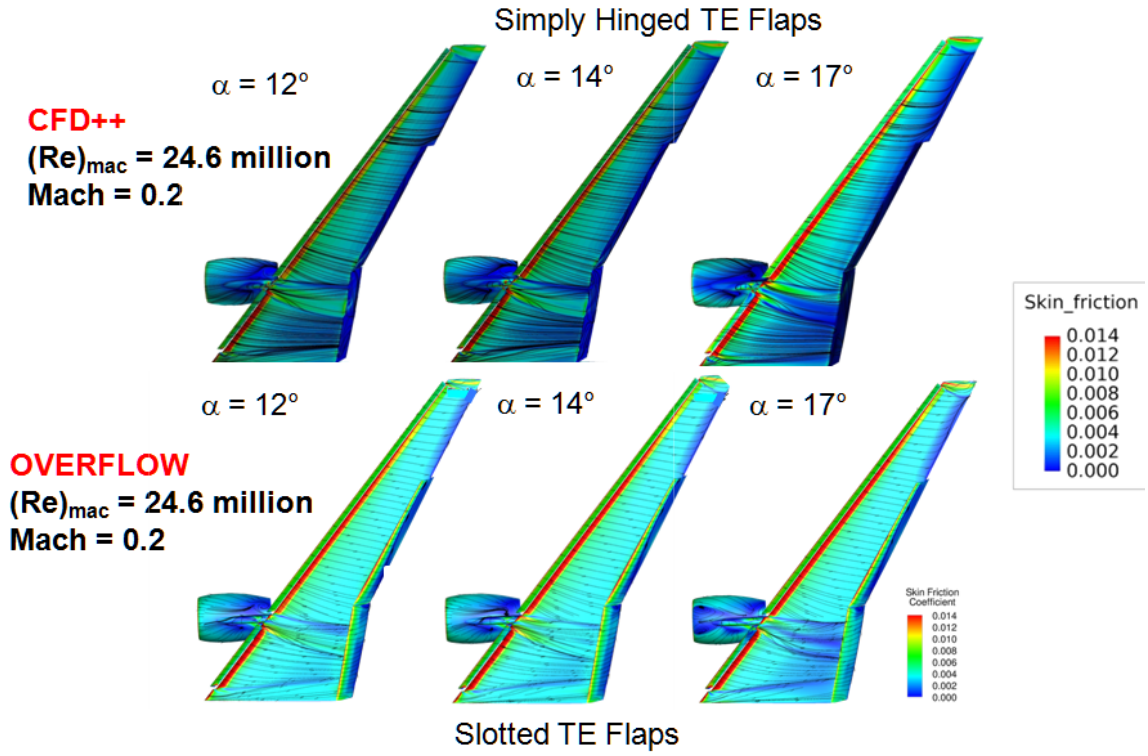

Figure 14 Surface streamlines and skin friction distribution for simplified and conventional HL-CRM in landing-approach configuration.

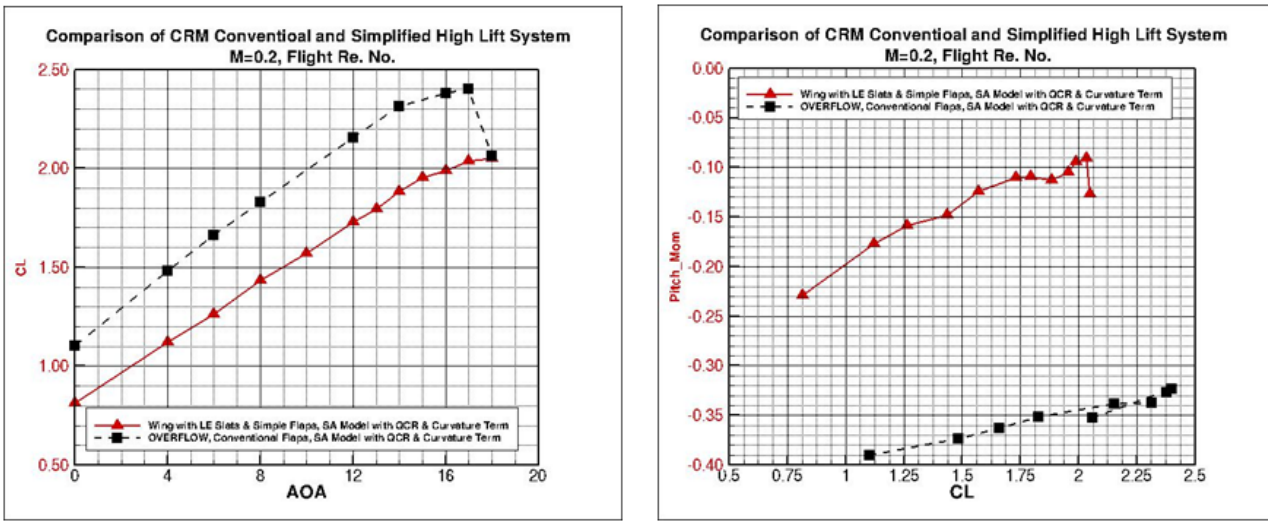

Figure 15 Forces and Moments for Upgraded AFC-Enhanced and for Refined Conventional High-Lift Common Research Model (CRM) Concept.

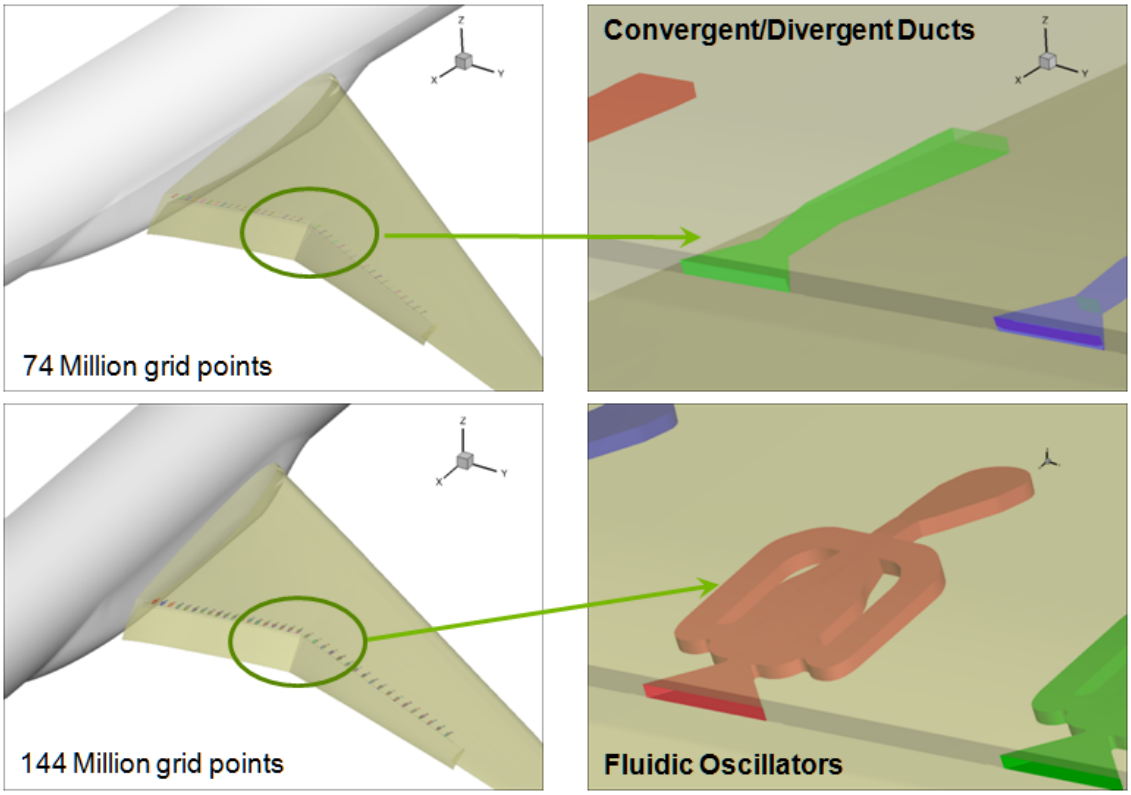

Figure 16 Replacing the convergent/divergent ducts for steady-flow AFC implementation with the more complex fluidic oscillators almost double the size of the computational grids

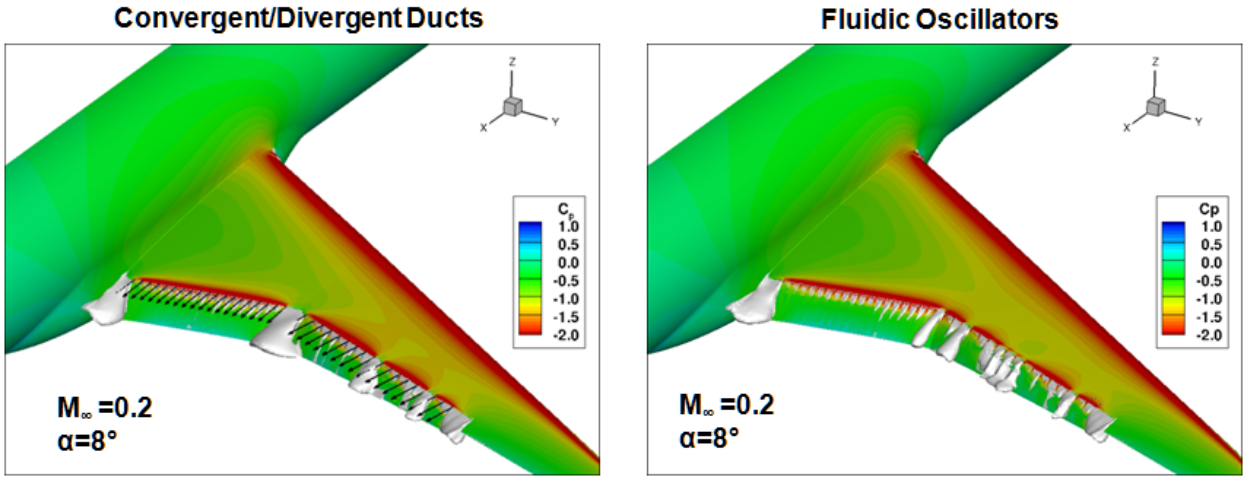

Figure 17 For comparable operating pressure ratios, fluidic oscillators and simple convergent/divergent ducts are comparably effective in controlling flow separation.

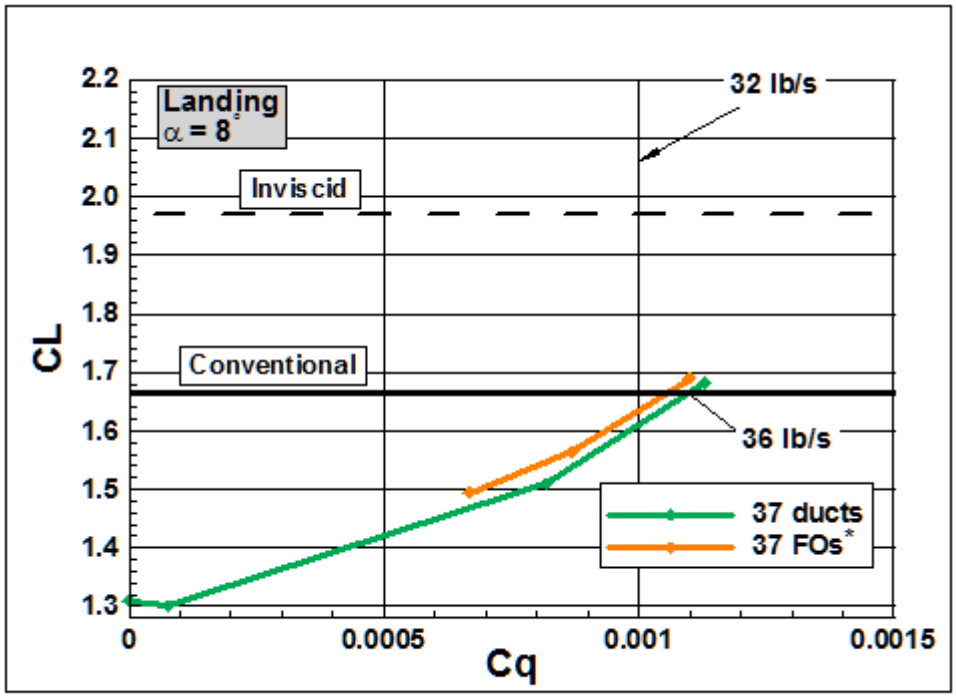

*FOs = Fluidic Oscillators

Figure 18 Fluid oscillators are slightly more effective than steady-flow AFC implementation through convergent/divergent ducts.

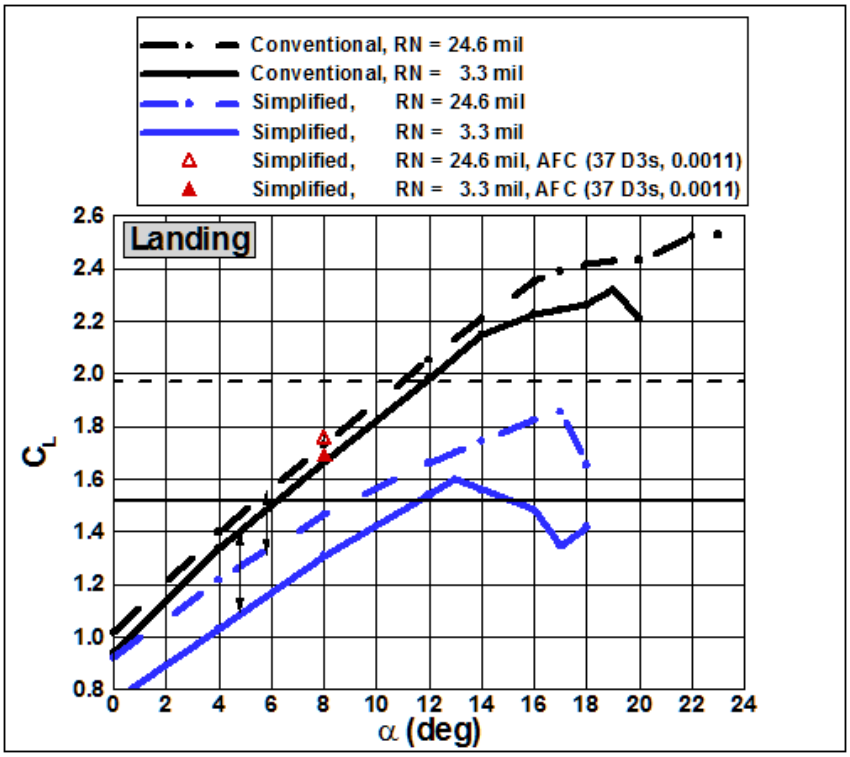

Figure 19 AFC actuation input shows little sensitivity to flight and wind-tunnel conditions

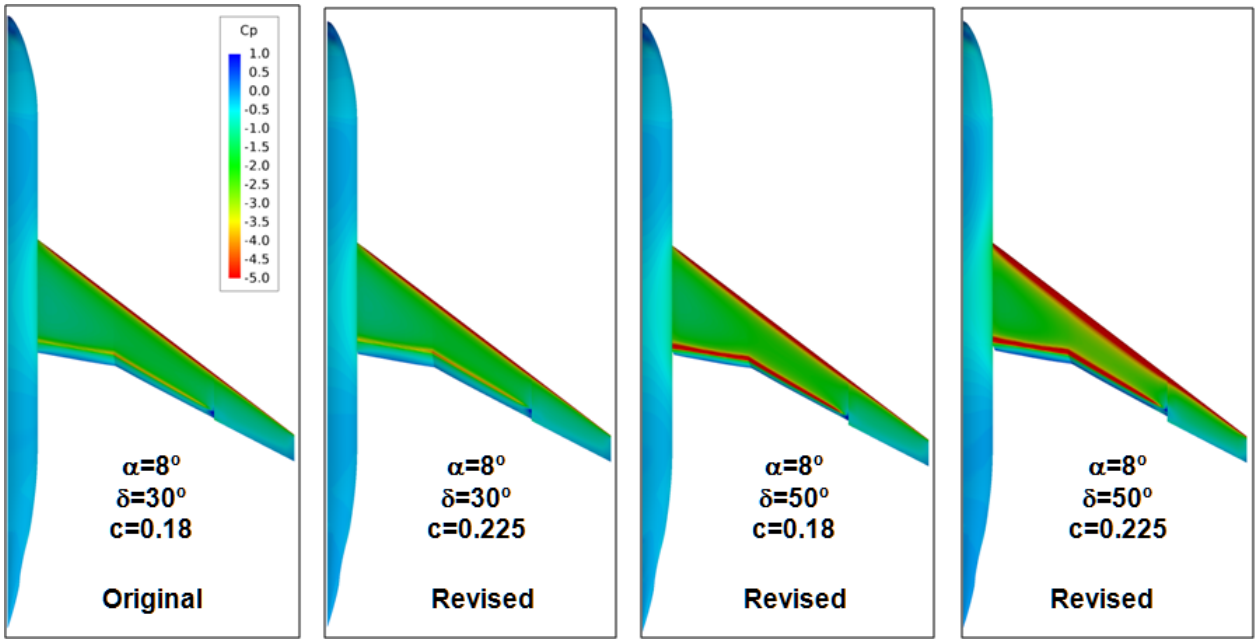

Figure 20 Linear potential flow solutions for simplified HL-CRM.v1 configuration indicate that trailing edge (TE) flap deflection has more effect on lift than TE chord.

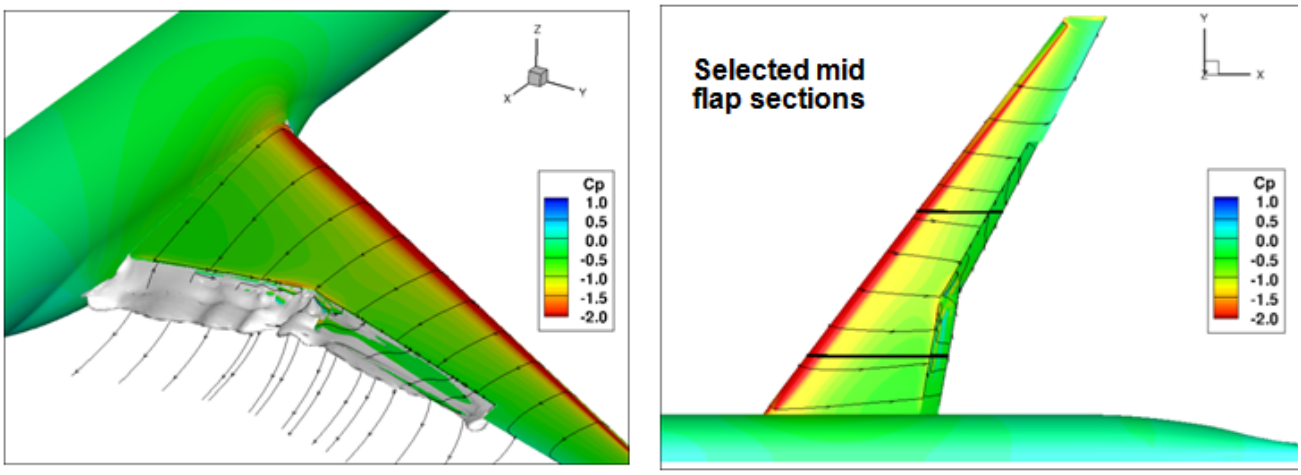

Figure 21 Moderate spanwise flow at flap hinge suggests that 2D analyses might provide guidelines for AFC implementation

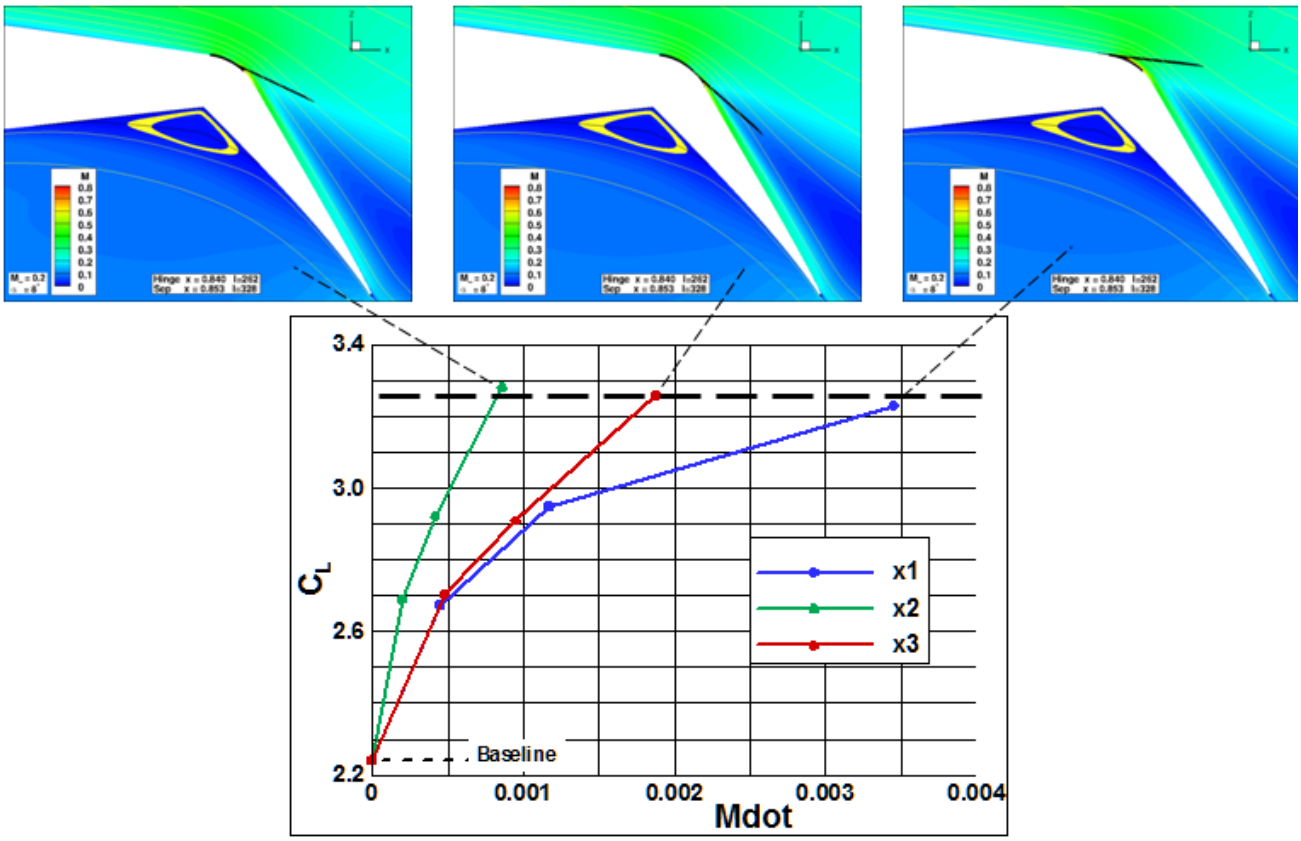

Figure 22 AFC jets are most effective when they are aligned with the local surface flow, and placement close to the separation point further improves flow control effectiveness

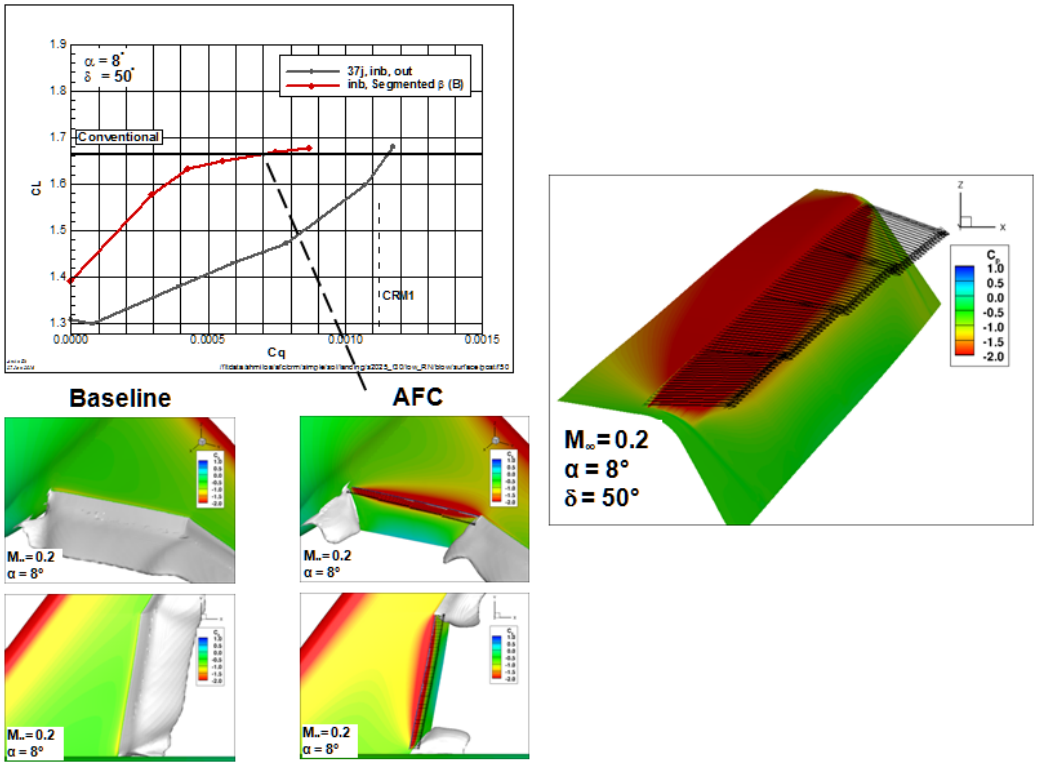

Figure 23 Inboard-flap-only applications of findings from parametric AFC integration study reduces AFC mass flow rate to 1/3 of phase-I study values.

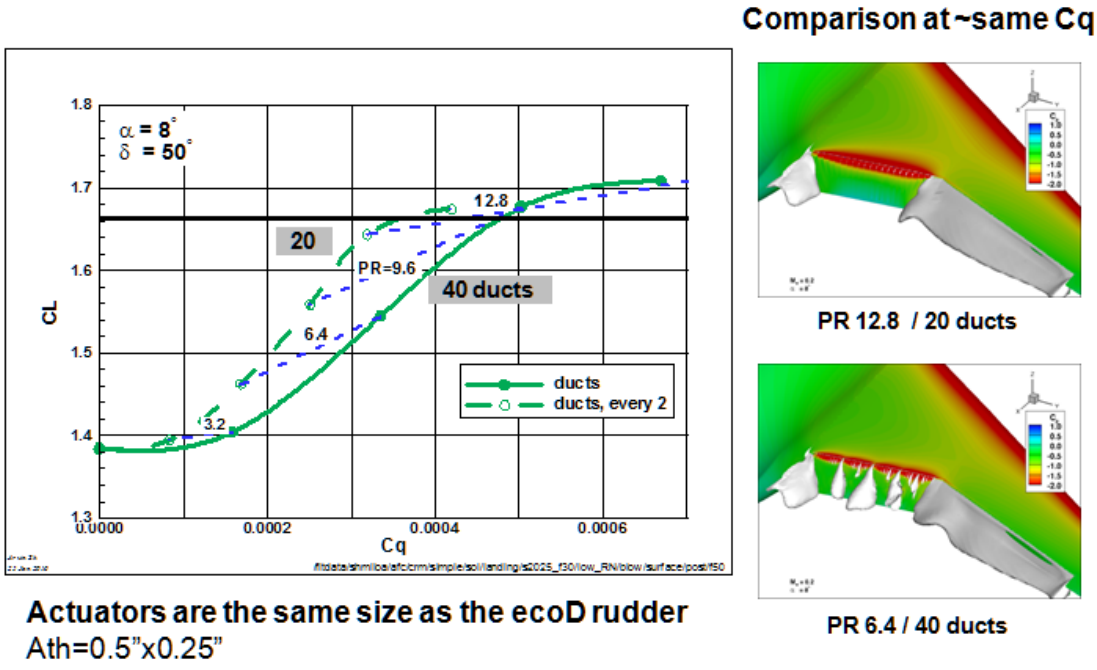

Figure 24 Effectiveness of AFC application through discrete duct arrays indicates that AFC mass flow is driver for AFC effectiveness, with AFC operating pressure about inversely proportional to number of AFC ducts.

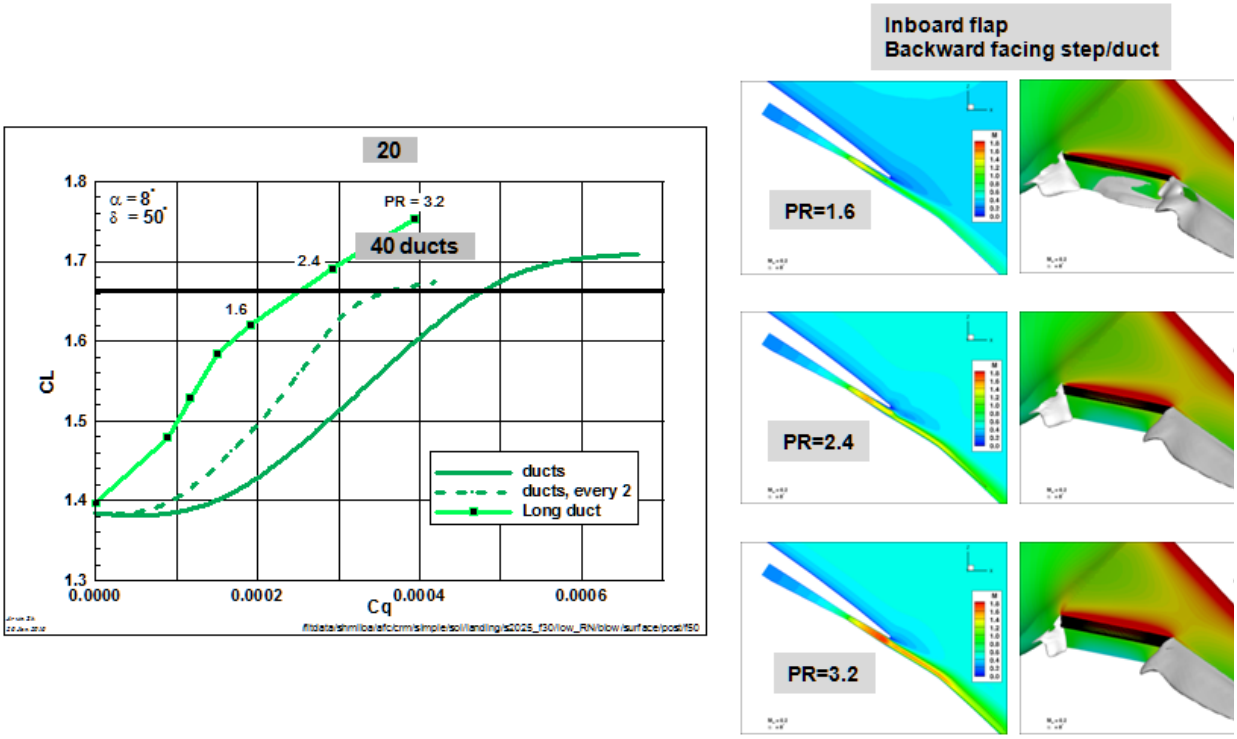

Figure 25 Continuous duct AFC concept is more efficient than discrete duct AFC concept as it requires less mass flow and lower operating pressures.

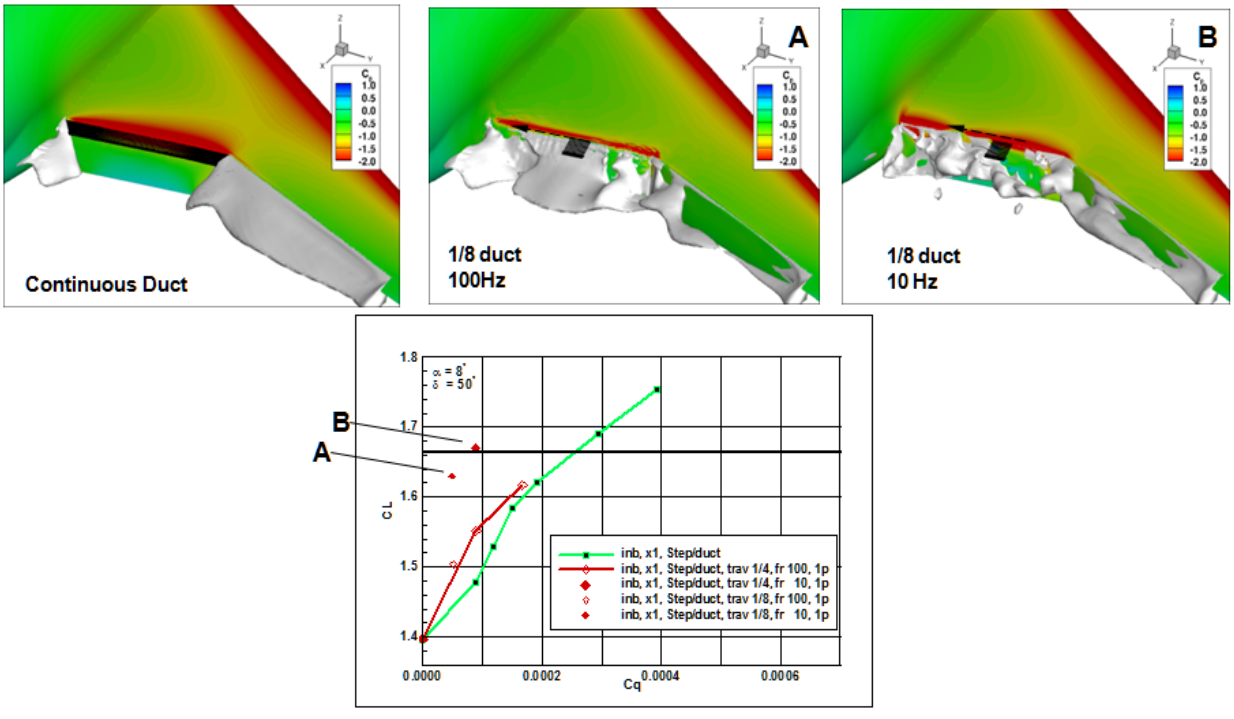

Figure 26 Traverse AFC concept reduces mass flow rate requirements by about an order of magnitude from the phase-I study values and reduces separated flow over both inboard and outboard trailing edge flaps.

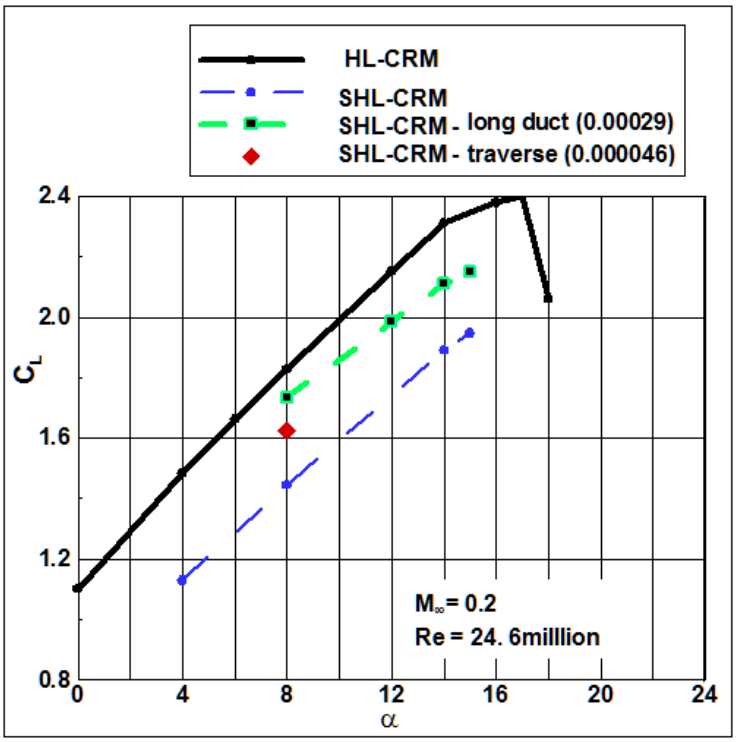

Figure 27 Initial AFC application to simplified HL-CRM concept significantly reduces the aerodynamic performance gap with conventional HL-CRM concept.

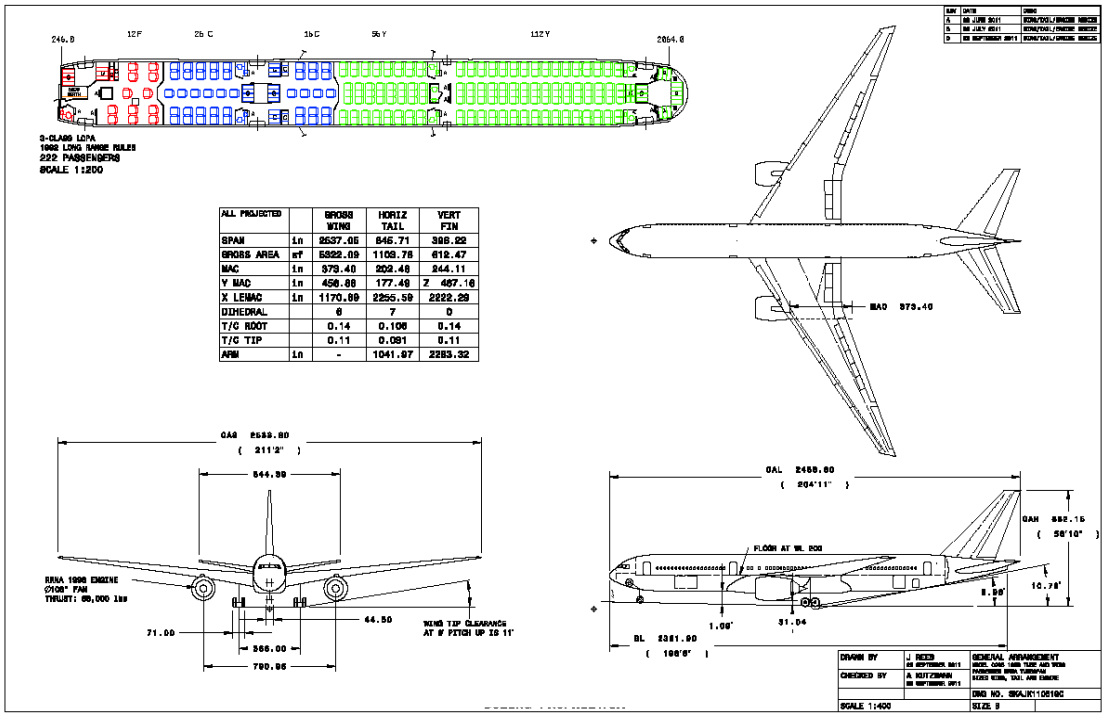

Figure 28 Trade studies are based on ERA-0003 concept which is a sized concept aircraft considered to be representative of CRM design.

Reference	Required Perf.	Baseline ERA-0003-PAX 1998 T&W Mcr=0.85 RR TF	AFC Enabled, Unsized TMFto=0.98 Unscaled Mcr=0.85 RR TF	AFC Enabled, Sized TMFto=0.98 Sized FN Mcr=0.85 RR TF	AFC Enabled, Sized TMFto=0.98 Sized FN and Swing Mcr=0.85 RR TF
MTOGW		582020	582020	576265	574907
OEW		268714	268743	267949	267494
Payload	50,000	50000	50000	50000	50000
Fuel at Max PL		263306	263277	258316	257413
Range (nm)	8000	8000	8117	8000	8000
Block Fuel Burned		238727	238805	234094	233361
Ton-nm/lbf		0.84	0.85	0.85	0.86
Wing Area, aero reference (sqft)		4960	4960	4960	5075
Aspect Ratio, aero reference		8.7222	8.7222	8.7222	8.7222
Span, aero reference (ft)		208.0	208.0	208.0	210.4
TO Ref FN @ SL, 0.0, +27F (lbf/eng)		88000	88000	88052	86065
Number of Engines		2	2	2	2
T/W		0.30	0.30	0.31	0.30
W/S		117	117	116	113
Optimum Altitude (ft)		36434	36352	36498	36713
Initial Cruise Thrust Ceiling (ft)		38341	38518	38702	38505
Initial Cruise Buffet Ceiling (ft)		41409	41396	41596	42138
Initial Cruise Altitude Capability (ft)		38341	38518	38702	38505
Cruise type		Step-Cruise	Step-cruise	Step-cruise	Step-cruise
Initial cruise altitude (ft)	35000	35000	35000	35000	35000
Top of climb thrust (all engines, tau=1)		35122	35122	35143	34350
Initial cruise Mach	0.85	0.85	0.85	0.85	0.85
Initial cruise L/D		19.373	19.651	19.615	19.615
Initial cruise SFC		0.5920	0.5921	0.5921	0.5921
Initial cruise tau		0.833	0.822	0.815	0.831
Initial cruise CL		0.4537	0.4540	0.4496	0.4381
Distance to climb (nm)	200	200	194	188	200
Takeoff field length @ SL, 86F (ft)	10500	8668	8862	8668	8668
2nd Segment Gradient (%)	2.4	2.518	2.465	2.504	2.529
Landing field length (ft)	5200	4032	4032	4025	3974
Approach speed (ktas)	150	108	108	108	107
			Range: +1.46% TOFL: +194 ft	Fuel Burn: -1.94%	Fuel Burn: -2.25%

Figure 29 Overall performance improvements due to AFC are primarily due to lower cruise drag.

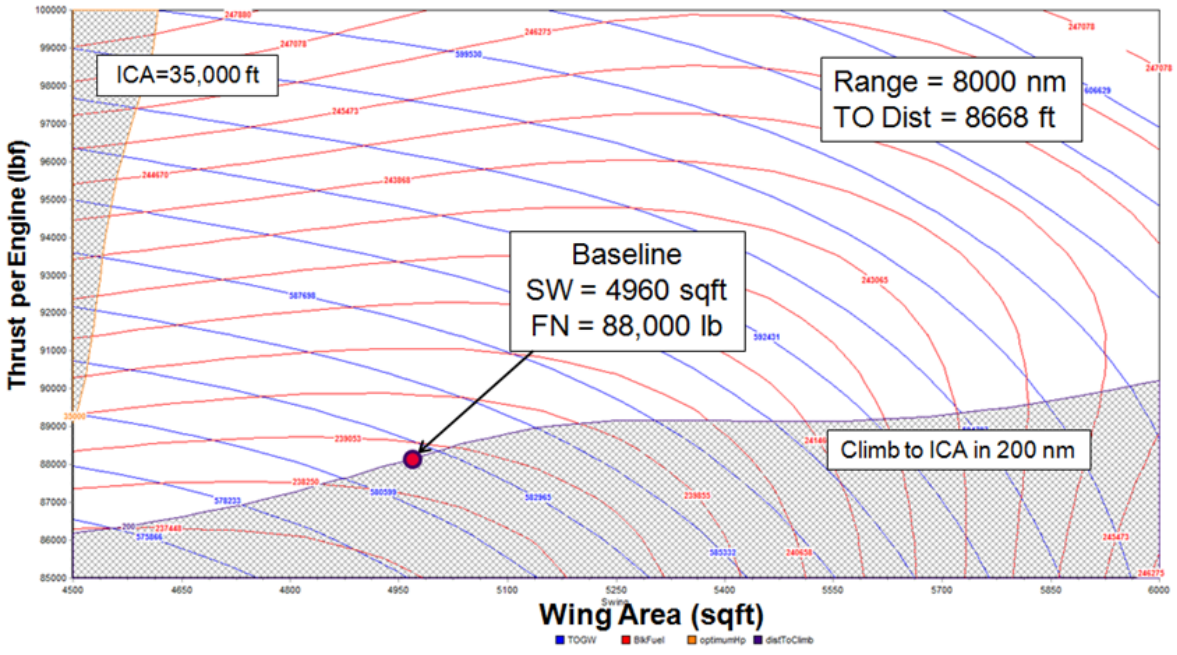

Figure 30 Climb-to-cruise requirement drives performance of baseline ERA-0003.

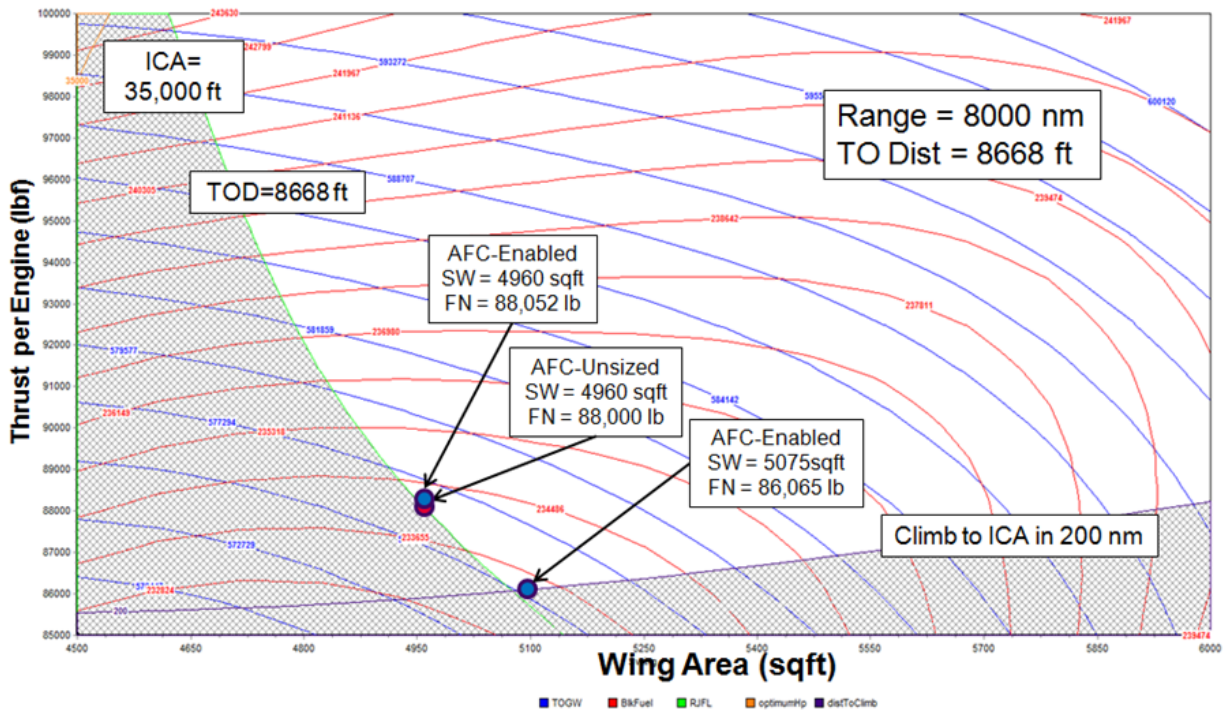

Figure 31 Resized AFC variants of ERA-0003 concept aircraft trade wing area and engine thrust to minimize fuel burn while meeting climb distance to initial cruise altitude and takeoff distance constraints.

REPORT DOCUMENTATION PAGE

Form Approved
OMB No. 0704-0188

1. REPORT DATE *(DD-MM-YYYY)*	2. REPORT TYPE	3. DATES COVERED *(From - To)*
01- 03 - 2016	Contractor Report	09/19/2014 - 01/29/2016

4. TITLE AND SUBTITLE

Refined AFC-Enabled High-Lift System Integration Study

5a. CONTRACT NUMBER

NNL10AA05B

5b. GRANT NUMBER

5c. PROGRAM ELEMENT NUMBER

6. AUTHOR(S)

Hartwich, Peter M.; Shmilovich, Arvin; Lacy, Douglas S. Dickey, Eric D.; Scalafani, Anthony J.; Sundaram, P.; Yadlin, Yoram

5d. PROJECT NUMBER

5e. TASK NUMBER

NNL14AB98T

5f. WORK UNIT NUMBER

081876.02.07.02.01.04

7. PERFORMING ORGANIZATION NAME(S) AND ADDRESS(ES)

NASA Langley Research Center
Hampton, Virginia 23681

8. PERFORMING ORGANIZATION REPORT NUMBER

9. SPONSORING/MONITORING AGENCY NAME(S) AND ADDRESS(ES)

National Aeronautics and Space Administration
Washington, DC 20546-0001

10. SPONSOR/MONITOR'S ACRONYM(S)

NASA

11. SPONSOR/MONITOR'S REPORT NUMBER(S)

NASA/CR-2016-219170

12. DISTRIBUTION/AVAILABILITY STATEMENT

Unclassified
Subject Category 34
Availability: NASA STI Program (757) 864-9658

13. SUPPLEMENTARY NOTES

Final Report

Langley Technical Monitor: John C. Lin

14. ABSTRACT

A prior trade study established the effectiveness of using Active Flow Control (AFC) for reducing the mechanical complexities associated with a modern high-lift system without sacrificing aerodynamic performance at low-speed flight conditions representative of takeoff and landing. The current technical report expands on this prior work in two ways: (1) a refined conventional high-lift system based on the NASA Common Research Model (CRM) is presented that is more representative of modern commercial transport aircraft in terms of stall characteristics and maximum Lift/Drag (L/D) ratios at takeoff and landing-approach flight conditions; and (2) the design trade space for AFC-enabled high-lift systems is expanded to explore a wider range of options for improving their efficiency.

15. SUBJECT TERMS

Active flow control; Commercial transport; Common research model; High lift; System integration

16. SECURITY CLASSIFICATION OF:			17. LIMITATION OF ABSTRACT	18. NUMBER OF PAGES	19a. NAME OF RESPONSIBLE PERSON
a. REPORT	b. ABSTRACT	c. THIS PAGE			STI Help Desk (email: help@sti.nasa.gov)
					19b. TELEPHONE NUMBER *(Include area code)*
U	U	U	UU	39	(757) 864-9658